Translational Oncology 15 (2022) 101240

Contents lists available at ScienceDirect

Translational Oncology

journal homepage: www.elsevier.com/locate/tranon

Original Research

Anti-GD2 CAR MSCs against metastatic Ewing's sarcoma

Giulia Golinelli [a,*], Giulia Grisendi [a,b], Massimiliano Dall'Ora [b], Giulia Casari [a], Carlotta Spano [b], Rebecca Talami [a], Federico Banchelli [c], Malvina Prapa [a], Chiara Chiavelli [a], Filippo Rossignoli [d,e], Olivia Candini [b], Roberto D'Amico [c], Milena Nasi [f], Andrea Cossarizza [g,h], Livio Casarini [i,j], Massimo Dominici [a,b,*]

[a] Division of Oncology, Department of Medical and Surgical Sciences for Children & Adults, University-Hospital of Modena and Reggio Emilia, Modena, Italy
[b] Rigenerand Srl, Medolla, Modena, Italy
[c] Center of Medical Statistic, Department of Medical and Surgical Sciences for Children and Adults, University-Hospital of Modena and Reggio Emilia, Modena, Italy
[d] Center for Stem Cell Therapeutics and Imaging (CSTI), Harvard Medical School, Boston, Massachusetts, United States of America
[e] Department of Neurosurgery, Brigham and Women's Hospital, Harvard Medical School, Boston, Massachusetts, United States of America
[f] Department of Surgery, Medicine, Dentistry and Morphological Sciences, University of Modena and Reggio Emilia, Modena, Italy
[g] Department of Medical and Surgical Sciences for Children and Adults, University of Modena and Reggio Emilia, Modena, Italy
[h] National Institute for Cardiovascular Research - INRC, Bologna, Italy
[i] Unit of Endocrinology, Department of Biomedical, Metabolic and Neural Sciences, University of Modena and Reggio Emilia, Modena, Italy
[j] Center for Genomic Research, University of Modena and Reggio Emilia, Modena, Italy

ARTICLE INFO

Keywords:
MSCs
TRAIL
GD2
Ewing's sarcoma
Metastatic model

ABSTRACT

Background: Ewing's sarcoma (ES) is an aggressive cancer affecting children and young adults. We pre-clinically demonstrated that mesenchymal stromal/stem cells (MSCs) can deliver tumour necrosis factor-related apoptosis-inducing ligand (TRAIL) against primary ES after local injection. However, ES is often metastatic calling for approaches able to support MSC targeting to the ES multiple remote sites. Considering that the disialoganglioside GD2 is expressed by ES and to optimise MSC tumour affinity, bi-functional (BF) MSCs expressing both TRAIL and a truncated anti-GD2 chimeric antigen receptor (GD2 tCAR) were generated and challenged against ES.
Methods: The anti-GD2 BF MSCs delivering a soluble variant of TRAIL (sTRAIL) were tested in several in vitro ES models. Tumour targeting and killing by BF MSCs was further investigated by a novel immunodeficient ES metastatic model characterized by different metastatic sites, including lungs, liver and bone, mimicking the deadly clinical scenario.
Findings: In vitro data revealed both tumour affinity and killing of BF MSCs. In vivo, GD2 tCAR molecule ameliorated the tumour targeting and persistence of BF MSCs counteracting ES in lungs but not in liver.
Interpretation: We here generated data on the potential effects of BF MSCs within a complex ES metastatic in vivo model, exploring also the biodistribution of MSCs. Our BF MSC-based strategy promises to pave the way for potential improvements in the therapeutic delivery of TRAIL for the treatment of metastatic ES and other deadly GD2-positive malignancies.

Research in context

Evidence before this study. Ewing's sarcoma (ES) mortality due to metastases and recurrent disease remains unacceptably high. Current evidence suggests that in patients with lung metastases or bone/bone marrow metastases or combined lung and bone/bone marrow metastases the use of aggressive local and systemic treatments improves outcome with variable degrees, whereas in presence of a more disseminated disease the outcomes are dismal. Novel therapies are necessary. Our group and others reported that ES is sensitive to apoptosis induced by the recombinant tumour necrosis factor-related apoptosis-inducing ligand (TRAIL), but the sub-optimal bioavailability of the drug prevented the introduction into clinical use. Using MSCs to improve the delivery of TRAIL showed efficacy in subcutis and orthotopic para-tibial models of ES. However, MSCs as TRAIL vehicle have not yet been explored

* Corresponding authors.
E-mail addresses: giulia.golinelli@unimore.it (G. Golinelli), massimo.dominici@unimore.it (M. Dominici).

https://doi.org/10.1016/j.tranon.2021.101240
Received 17 June 2021; Received in revised form 28 September 2021; Accepted 5 October 2021
Available online 12 October 2021

for metastatic ES. The ganglioside GD2 is a potential cell surface target for cell-based approaches to treat ES.

Added value of this study. In this study, we propose a strategy where a soluble form of TRAIL (sTRAIL) is delivered by MSCs that are also modified to express an anti-GD2 receptor (GD2 tCAR). These bi-functional (BF) MSCs combine the higher tumour affinity conferred by the expression of GD2 tCAR with the capacity to target distant tumour cells through the release of sTRAIL. In the in vivo ES metastatic model, BF MSCs were able to counteract tumour growth in the lungs, whereas producing a slight, though not significant, antitumour effect on liver metastases compared with the control groups. The presence of GD2 tCAR on BF MSCs appeared to strengthen the binding to metastases, resulting in an increase in the tumour-associated MSC signal which was detected early in the lungs. At later time points, we observed a tendency of GD2 tCAR to improve the retention of BF MSCs in the liver.

Implications of all the available evidence. Our study produced relevant information with translational impacts aimed at identifying novel therapeutic strategies for the potential treatment of high-stage ES and other deadly GD2-positive malignancies. With the limitation of a single cell therapy strategy, we provided insights regarding the potential effects of BF MSCs within a complex ES metastatic model, exploring also MSC fates in vivo. These results warrant further investigations regarding the optimal cell dose and schedule, together with the possibility of introducing combinatory approaches with other anticancer agents.

Introduction

Ewing's sarcoma (ES) is an aggressive tumour that can arise in either bone or soft tissues representing the second-most-common bone cancer among children and young adults [1]. Initially, ES cells were believed to be derived from primitive neuroectodermal cells because they express early neuronal markers. More recently, several studies converged on mesenchymal stromal/stem cells (MSCs) as cells of origin for ES [2,3]. Despite marked improvements in the prognosis of patients with localised ES, mortality due to metastases and recurrent disease remains unacceptably high, with survival rates ranging from 29% to 52% in those with isolated lung metastases, lower survival rates reported for those with bone/bone marrow metastases and even worse in presence of an extensive, multiorgan-disseminated disease [4–6]. Although approximately 25% of patients present with gross metastases, ES is associated with a subclinical micrometastatic spread, which is responsible for the high relapse rate [1]. Currently, an urgent and unmet need exists for the development of novel treatment strategies to improve the outcomes of metastatic and recurrent ES, including targeted therapies and immunotherapies [1,7].

New avenues of research have been opened through the use of the anticancer agent tumour necrosis factor-related apoptosis-inducing ligand (TRAIL). Recombinant human TRAIL (rhTRAIL) has shown promising effects against most cancers but its suboptimal bioavailability due to rapid clearance, as well as its weak capacity to induce the efficient clustering of TRAIL receptors have prevented its development for clinical use [8–10]. Among the many potential strategies for increasing the therapeutic effects of TRAIL, the use of cells that express TRAIL looks promising [11]. MSCs have been identified as suitable vehicles for the delivery of anticancer molecules to tumour sites, including TRAIL [12–18].

We demonstrated that MSCs engineered to express a membrane-bound form of TRAIL (mTRAIL) induce apoptosis in a variety of sarcomas, exerting relevant antitumour activity in a subcutaneous ES model [16]. These findings were further confirmed by our group and others in different para-tibial orthotopic ES models [19]. However, metastases represent a great challenge in ES patients; therefore, dedicated strategies designed to target MSCs to metastatic sites in ES, particularly the lungs, and to increase the in vivo persistence of MSCs remain necessary. A high level of MSC engraftment in the lung after systemic infusion, combined with novel targeting properties induced by gene modifications, could represent a novel and effective approach to treat ES, even after metastatic dissemination [13,20–24].

The disialoganglioside GD2 is a surface molecule expressed at high levels by a wide range of tumours, with restricted and low expression levels in normal tissues [25,26]. GD2 has also been localised in ES cell lines and primary ES samples [27,28]. GD2 expression has been reported to be a common feature of ES, based on tissue biopsies from patients at various ES stages and during relapse [29]. As a glycosphingolipid antigen, GD2 is not presented to T cells by the major histocompatibility complex (MHC) class I. T cell engagement by GD2 has become possible through the use of chimeric antigen receptor (CAR) T cell immunotherapy [29,30]. Despite promising in vitro results, CAR-modified T or natural killer (NK) cells used as monotherapies failed to control tumour growth in various metastatic ES models [31,32]. As for other solid tumours, GD2 CAR T cell failure could be explained by the presence of immunoinhibitory signals in the tumour microenvironment, which tolerise T cells and render them dysfunctional against the targeted tumour [33]. A synergistic inhibition of metastatic disease has been achieved by Charan et al. through the combination of GD2-specific CAR T cell therapy with hepatocyte growth factor (HGF) receptor-neutralising antibody [34]. Affinity-based cell targeting has also been applied to MSCs. Tumour-specific targeting and retention were achieved by the genetic modification of MSCs using artificial receptors designed to bind specifically with glioblastoma (GBM) and ovarian cancer cells [35,36]. Recently, we proposed a bi-functional (BF) approach, in which anticancer molecule delivery is mediated by cells that simultaneously express a CAR [37]. These BF MSCs co-express TRAIL and a truncated CAR targeting GD2 (GD2 tCAR) and can be used as a new tool for the treatment of GD2-positive tumours. The developed GD2 tCAR has been introduced to MSCs aiming for a specific and prolonged retention of MSCs at GD2-expressing tumour sites, providing a more effective delivery of TRAIL. Proof of concept for this technology has been generated in the highly GD2-positive GBM using BF MSCs expressing mTRAIL [37]. In that context, we demonstrated that the functionalisation of MSCs using GD2 tCAR could force an interaction between BF MSCs and GBM cells expressing the GD2 surface antigen. Here, BF MSCs have been armed with GD2 tCAR together with a soluble variant of TRAIL (sTRAIL), previously tested against pancreatic cancer, to develop a more powerful MSC-based therapeutic strategy for the treatment of metastatic ES [17,18]. These BF MSCs combine the higher tumour affinity conferred by the expression of GD2 tCAR with the capacity to target distant tumour cells through the release of sTRAIL. To challenge BF MSCs, we generated an in vivo model in NSG mice that rapidly and closely reflects the clinical scenario of widely disseminated ES [1]. Our study generates translational impacts aimed at identifying novel therapeutic strategies for the potential treatment of metastatic ES and ultimately for still deadly GD2-positive malignancies, like osteosarcoma, melanoma, neuroblastoma, glioma and small cell lung cancer [26].

Material and methods

Cell cultures and maintenance

The human ES cell lines TC71 (RRID: CVCL_2213, DSMZ, Braunschweig, Germany) and A673 (kind gift from Dr. Nicola Baldini, Rizzoli Orthopaedic Institute, Bologna, Italy) were cultivated in Iscove's modified Dulbecco's medium (IMDM, Euroclone, Milan, Italy). RD-ES cell line (RRID: CVCL_2169, ATCC, LGC Standards S.r.l., Milan, Italy) was maintained in RPMI 1640 (Gibco, Thermo Fisher Scientific, Waltham, Massachusetts, USA). Media were supplemented with 10% FBS (Carlo Erba Reagents Srl, Cornaredo, Italy), 1% L-glutamine (200 mM; BioWhittaker, Lonza, Verviers, Belgium), and 1% penicillin-streptomycin (10^4 UI/ml penicillin and 10 mg streptomycin/ml; Carlo Erba Reagents Srl). Human adipose (AD)-MSCs were isolated from

healthy donors ($n = 2$) as previously described [14]. After isolation, cells were grown in minimal essential medium with alpha modifications (α-MEM, Gibco) containing up to 5% platelet lysate (PL, Macopharma, Tourcoing, France), 1% L-glutamine, 0.5% ciprofloxacin (Fresenius Kabi Italia S.r.l., Verona, Italy), and 0.2% heparin (Sigma-Aldrich, Saint Louis, Missouri, USA). Cells were incubated and maintained within a controlled atmosphere with 5% CO_2 and a temperature of 37 °C. The authentication of TC71, A673, and RD-ES cell lines was recently performed by the Leibniz Institute DSMZ - German Collection of Microorganisms and Cell Cultures GmbH.

Viral vectors and cell transduction

We recently generated a truncated CAR (tCAR) able to bind the disialoganglioside GD2 for use in affinity-based targeting approaches against GD2-expressing cancers [37]. The truncated anti-GD2 CAR (GD2 tCAR) is composed by an anti-GD2 single-chain variable fragment (scFv) from a murine antibody of IgM class linked to a portion of CD8, the CD8α hinge-transmembrane domain, and lacks the signalling domains 4–1BB (CD137) and CD3-ζ of the original anti-GD2 CAR [25,37]. The GD2 tCAR expression cassette was cloned into the lentiviral vector pCCL PGK WPRE for the gene modification of AD-MSCs, resulting in the surface expression of GD2 tCAR (Fig. 1a, first row). A gene encoding a soluble trimeric TRAIL variant was cloned into the pCCL PGK or MND WPRE vectors, which was used to engineer AD-MSCs that release the sTRAIL molecule, as previously described (Fig. 1a, second row) [17]. MSC transduction was performed as reported [38]. The obtained MSC lines were defined as transduced with an empty vector (EV MSCs), transduced with the GD2 tCAR vector (GD2 tCAR MSCs), transduced with a vector carrying sTRAIL alone (sTRAIL MSCs), and transduced with both the GD2 tCAR and sTRAIL vectors (BF MSCs). Gene-modified MSCs were used from P8 to P13. The MIGR1 vector, which encoded the red fluorescent protein DsRed, was used to stably transduce ES cell lines (TC71 and A673) to facilitate the distinction of ES cells from MSCs in cell-to-cell interaction assays and spheroid models. Retrovirus production was performed using the FLYRD18 packaging cell line (RRID: CVCL_8871), as previously described [16,39]. The TC71 ES line was engineered to express a red-shifted *Luciola italica* luciferase transgene using RediFect™ Red-FLuc-Puromycin Lentiviral Particles (PerkinElmer, Waltham, Massachusetts, USA), according to the manufacturer's instructions. Photon emissions from the obtained luciferase-expressing TC71 (TC71 Luc) cells were measured using the IVIS Lumina XRMS (IVIS Lumina XRMS *In Vivo* Imaging System, PerkinElmer) with Living Image software (version 4.3.1, PerkinElmer), which was used to estimate the level of photon emission per cell.

FACS on gene modified MSCs

The TRAIL presence on MSC surface was assayed by fluorescence-activated cell sorting (FACS) using a phycoerythrin (PE)-conjugated anti-TRAIL antibody (Cat. No. 308206, RRID: AB_2205825, BioLegend, San Diego, California, USA). The intracellular staining of transduced MSCs was performed with a Becton Dickinson Cytofix/Cytoperm kit (BD, Franklin Lakes, New Jersey, USA). To detect GD2 tCAR expression on MSCs, anti-idiotypic antibodies were generated as previously described [25,40]. MSCs were incubated with anti-idiotype mouse sera followed by allophycocyanin (APC)-conjugated goat anti-mouse secondary antibody (Cat. No. 550826, RRID: AB_398465 BD). The corresponding isotype-matched antibodies were used as negative controls (provided by BD and BioLegend). Data were collected using a FACS Aria III flow cytometer (BD) and analysed using FACS Diva software (BD).

Cell-to-cell interaction assays

The affinity-based recognition of ES cell lines by GD2 tCAR-functionalised MSCs was investigated using cell-to-cell interaction assays, as previously described [37]. ES cell lines (TC71 and A673) expressing DsRed were used. The RD-ES cell line was labelled using the CellTracker Deep Red dye (Thermo Fisher Scientific). Similarly, MSCs were labelled with a carboxyfluorescein succinimidyl ester (CFSE, Molecular Probes, Eugene, Oregon, USA) fluorescent dye, according to the manual supplied with the reagent. The absolute number of MSC-tumour cell aggregates was quantified by FACS by measuring the CFSE/DsRed (or Deep Red) double-positive population within a 60-second window. The number of MSC-tumour cell aggregates acquired for each tested condition was compared with the number acquired for EV MSCs and the data were presented as the fold change. The stability of the GD2 tCAR-mediated binding was further evaluated by comparing interactions with TC71 cells between EV MSCs and GD2 tCAR MSCs. After detachment with trypsin, MSC-TC71 cell aggregates were maintained in non-permissive conditions at 4 °C on a rotating support for 2 or 4 h, and the absolute number of aggregates was quantified by FACS. The number of aggregates at 2 or 4 h was compared with the respective baseline value collected at the detachment time point (T0) and the data were presented as the fold change.

Collection of sTRAIL-containing supernatants

Conditioned SNs from MSCs secreting sTRAIL were produced as follows. Briefly, when MSCs reached almost 80% confluence, the maintenance PL-based medium was replaced with the tumour culture medium for the tumour cell line of interest. After 48 h, conditioned SNs were collected, filtered through a 0.22-μm filter (Euroclone), and stored at −80 °C until use. SNs from EV and GD2 tCAR MSCs were collected for use as controls.

Cytotoxicity assays

Cell-mediated cytotoxicity by two-dimensional (2D) co-culture: all gene-modified MSCs were labelled with CFSE cell tracker (Molecular Probes) and seeded in a 12-well cell culture plate (Corning). After 12 h, tumour cell lines were co-cultured at different target to effector (T:E) ratios (1:1, 1:2, and 1:5). The tumoricidal activity of MSCs was evaluated by PI staining after 24 h by FACS gating on CFSE-negative cells and PI-positive events. sTRAIL-mediated cytotoxicity by 2D assay: to assess sTRAIL-mediated cytotoxicity, tumour cells were seeded in a 12-well cell culture plate at 6 000 cells/cm^2. The following day, the cells were incubated for 24 h with SNs collected from MSCs. The death rate was assessed by FACS using PI staining. Cell-mediated cytotoxicity by the three-dimensional (3D) spheroid model: DsRed-expressing tumour cell lines were seeded at 20 000 cells/well in 96-well ultra-low attachment plates (Corning), enabling the formation and growth of a single spheroid per well with a reproducible size. After 24 h, all gene-modified MSCs were labelled with CFSE and added at a 1:1 T:E ratio. The co-culture was followed by fluorescence microscopy. The tumoricidal activity of MSCs was evaluated after 15 h using two bioluminescence assays and the GloMax® Discover plate reader (Promega). The CellTiter-Glo® (Promega) assay, an ATP detection assay designed to measure the viability of 3D microtissue, and the Caspase-Glo® 8 assay (Promega), which measures caspase-8 activity. After 2 days, representative spheroids were embedded in OCT (VWR, Radnor, Pennsylvania, USA) and frozen sections were collected using a cryostat (Leica, Wetzlar, Germany). Cell-mediated cytotoxicity by the 3Dmatrix model: TC71 Luc cells were seeded at a cell number of 140 000 cells on a 3D fibre-based matrix, composed of an inert and biocompatible synthetic polyester with a thickness of 400 μm. MSCs were added after 12 h at a T:E ratio of 3:1. MSC-mediated toxicity was assessed in a time course co-culture (15, 24, and 48 h) and an endpoint assay after 4 days. The bioluminescent signal after luciferin (XenoLight D-Luciferin-K+ Salt; PerkinElmer) administration was quantified using the GloMax® Discover plate reader (Promega) as a measure of tumour cell viability on the matrix. In all cytotoxicity assays, rhTRAIL at 1 μg/ml was used as a positive control,

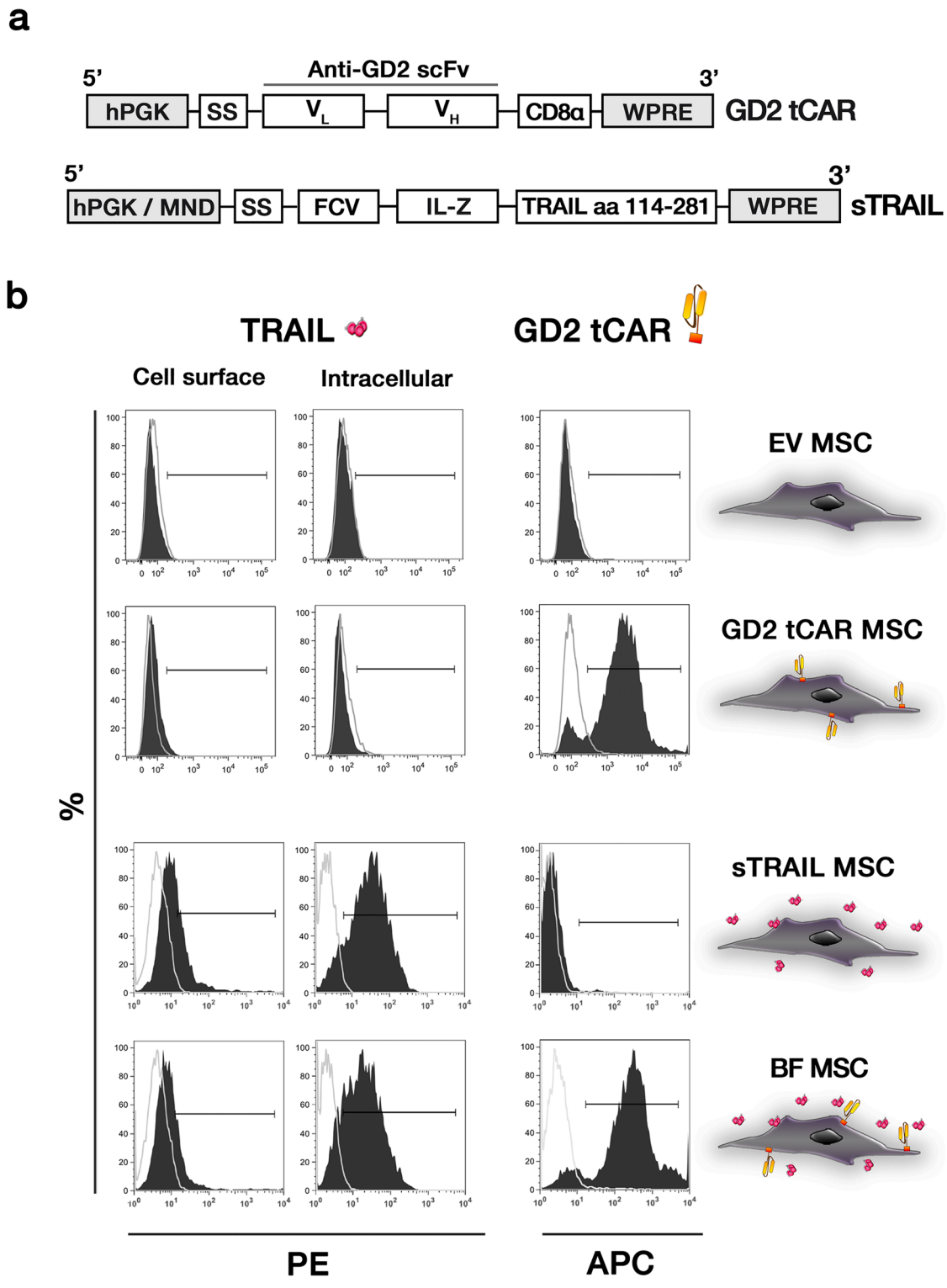

Fig. 1. MSCs can be effectively transduced with GD2 tCAR and/or TRAIL encoding vectors. **a**, Schematic presentation showing the GD2 tCAR expression construct (upper), in which the IgM derived anti-GD2 scFv was fused with the human CD8α-derived hinge-transmembrane domain, and the sTRAIL expression construct (lower), in which an immunoglobulin secretion sequence (SS), the human stromelysin-3 furin-specific cleavage site (FCV), and the yeast GCN4 isoleucine zipper trimer forming domain (IL-Z) were combined with the TRAIL receptor binding domain sequence (amino acids 114–281). **b**, FACS analysis of TRAIL and GD2 tCAR expression on EV MSCs transduced with empty vector (first row), GD2 tCAR MSCs transduced with the GD2 tCAR vector (second row), sTRAIL MSCs transduced with the vector encoding sTRAIL (third row), and BF MSCs transduced with the vectors for both GD2 tCAR and sTRAIL (fourth row).

and TC71 cells alone (CTR) were used as a negative control.

In vivo studies

Animal models of metastatic ES were attempted in hairless SCID (SHO-Prkdc^{scid}Hr^{hr}, RRID: IMSR_CRL:474), NOD SCID (NOD.CB17-Prkdc^{scid}/J) and NSG (NOD.Cg-Prkdc^{scid} Il2rg^{tm1Wjl}/SzJ, RRID: BCBC_4142) mice infusing between 1 million-2 million of TC71 Luc cells.

EV and GD2 tCAR MSCs were genetically modified with a pCCL PGK WPRE lentiviral vector encoding green fluorescent protein (GFP), as previously reported [38]. aAmong the tested strains, the NSG were specifically considered in the therapeutic model. Thus, a total of 62 female and male 8–10-week-old NSG mice were obtained from Charles River (Charles River Laboratories Italia Srl, Lecco, Italy) and housed under a 12 h light, 12 h dark cycle with no restrictions on food and water. Sample size was estimated using the software G* Power version 3.1.9.2 (Heinrich-Heine-University, Düsseldorf, Germany). Mice were fed with a Teklad global purified rodent diet (2016) (Envigo, Indianapolis, Indiana, USA) to reduce any potential signal interference from food during imaging analyses. NSG animals were intravenously (i.v.) inoculated with 2 million TC71 Luc cells suspended in 150 µl phosphate-buffered saline (PBS). Four days after tumour cell inoculation, the animals were randomly divided into five groups for treatment: the control group (CTR, $n = 22$) received no treatment (150 µl PBS); the EV MSC ($n = 10$), GD2 tCAR MSC ($n = 10$), sTRAIL MSC ($n = 10$), and BF MSC ($n = 10$) groups each received multiple ($n = 3$) i.v. injections consisting of 1 million of the respective gene-modified MSCs, which were administered every 3 days in 150 µl PBS. For the third injection, the MSCs were labelled with XenoLight DiR (8 µM; Perkin Elmer), following the manufacturer's instructions. DiR is a near-infrared fluorescent dye (Absorbance/Emission: 748/780 nm), which allowed us to track MSC fates in vivo. The absence of mycoplasma contamination was verified in inoculated cells before in vivo use with a MycoAlert Mycoplasma Detection Kit (Lonza, Verviers, Belgium). Starting from day 1 post-injection, the animals' health was monitored regularly, and weight was measured weekly. Animals were recurrently imaged using the IVIS Lumina XRMS to detect the bioluminescent signal from TC71 Luc cells and the DiR fluorescence of MSCs. Prior to imaging, the skin over the abdomen was depilated with Veet cream (Reckitt Benckiser Healthcare, Milano, Italy). For bioluminescence detection, 12 min after the subcutaneous injection of 150 mg/kg luciferin solution, the animals were anaesthetised with isoflurane (Merial, Lione, France) and imaged. DiR fluorescence was recorded by imaging the mice with the IVIS at the appropriate excitation and emission spectra. Fixed regions of interest (ROIs) were drawn around the lungs, liver, and full body, and the total radiant efficiency [p/s/cm^2 /sr] / [µW]/cm^2] of DiR fluorescence was quantified using Living Image software (Perkin Elmer). Intra-group analyses of DiR fluorescence over time were performed using total radiant efficiency for the lung and liver ROIs. To compare different mouse groups in terms of the relative distribution of MSCs in the lungs and liver, the total radiant efficiency of the lungs (or liver) was normalised against that for the full body, and the ratio was expressed as a percentage. Normalisation avoids the potential that intergroup comparison might be affected by slight differences in the DiR labelling of gene-modified MSCS. The median and interquartile range (IQR) values were calculated and compared between groups. X-ray image acquisitions were overlaid on both optical and photographic images, providing anatomical context to the bioluminescence and fluorescence signals. After 13 days, animals were sacrificed by the intraperitoneal injection of Tanax (Intervet Italia Srl, Milano, Italy), and the organs (lungs, liver, and femur) were examined for the presence of metastases using IVIS. ROIs were manually drawn around metastases, and the total photon flux [p/s] emitted from tumour cells was quantified using Living Image software. Organs were then preserved for molecular and histologic evaluation.

Droplet digital PCR (ddPCR)

The lungs and liver were extracted, maintained on dry ice, and stored at −80 °C. Frozen organs were placed into gentleMACS M Tubes (Miltenyi, Bergisch Gladbach, Germany) and homogenised in Tissue Lysis Buffer (TLA; Promega) using gentleMACS Dissociators (Miltenyi). After centrifugation at 200 g for 2 min, the homogenate was collected and incubated with proteinase K (2 mg/ml; Promega) at 56 °C for 30 min. The lysate was carefully mixed, and a representative fraction was sampled for genomic DNA (gDNA) extraction. gDNA was automatically isolated using a Maxwell 16 Instrument (Promega) using the Maxwell 16 LEV Blood DNA Kit (Promega), according to the manufacturer's instructions. Contaminating RNA was removed by the addition of RNase (20 µg/ml; Promega) to the elution buffer. The gDNA concentration was measured using the Infinite M Nano (Tecan, Männedorf, Zürich, Switzerland), and gDNA samples were diluted to approximately 40 ng/µl. Custom primers and probes conjugated to 6-carboxyfluorescein (FAM) were designed to target selected genes using the Primer3Plus Web interface (Supplementary Table S1) and produced by Bio-Rad (Hercules, California, USA). The Luc assay was designed to target the luciferase gene and was used to detect TC71 Luc tumour cells. The GFP assay was designed to target the GFP gene for the detection of EV MSCs or GD2 tCAR MSCs. The sTRAIL assay was designed to target the sTRAIL gene and was used to assess sTRAIL MSCs or BF MSCs. The human ribonuclease P/MRP subunit P30 gene (hRPP30; AssayID: dHsaCP2500350, Bio-Rad) and the *Mus musculus* transferrin receptor gene (mTfrc; AssayID: dMmuCNS420644255, Bio-Rad) reference assays, which were both conjugated with hexachlorofluorescein (HEX), were used for human and murine cell detection, respectively, and for gene copy number (CN) analysis. The absolute quantification of each target and reference gene was performed using the QX200 ddPCR System (Bio-Rad). Briefly, the ddPCR mixture was composed of extracted gDNA, the target and reference primers and probes, 4x ddPCR Multiplex Supermix for Probes (Bio-Rad), DTT (4 mM; Thermo Fisher Scientific), and nuclease-free water (Thermo Fisher Scientific). The ddPCR reaction mixture was partitioned into droplets and cycled with the following conditions: 95 °C for 10 min (1 cycle); 94 °C for 30 s and 55 °C for 2 min (37 cycles), with a ramp of 2 °C/s; 98 °C for 10 min (1 cycle), and 4 °C hold for at least 2 h. Data analysis was performed by QuantaSoft Software (Version 1.5.38, Bio-Rad). Positive droplets containing amplification products were discriminated from negative droplets without amplification products. The concentration (copies/µl) of each target and reference gene was reported automatically by QuantaSoft Software. gDNAs isolated from TC71 Luc cells and gene-modified MSCs were first used to estimate the CN of the target genes using 2-plex ddPCR assays in which the assay for the target gene is combined with the hRPP30 reference assay, at a final concentration of 900 nM primers/250 nM probe. The ratio between the target and reference concentrations was multiplied by the reference CN per genome (two for diploid genomes) to calculate the target gene CN. The restriction digestion of gDNAs was further performed to exclude potential errors in CN estimation related to the presence of potentially linked tandem genes. The HpyCH4V restriction enzyme (New England BioLabs, Ipswich, Massachusetts, USA) was selected as being capable of digesting upstream and downstream of every target gene, producing fragments of 200–300 bp, without cutting the amplicons of either target or reference genes. The direct digestion of gDNA samples (25 ng) was performed by adding HpyCH4V (2 units) to the ddPCR reaction mixture. The digestion of gDNA prior to the addition to ddPCR was also assessed. Approximately 500 ng of gDNA was digested with 7.5 units of the restriction enzyme HpyCH4V for 1 hour at 37 °C, with subsequent heat-inactivation at 65 °C for 20 min. Then, 25 ng of the digested gDNA was used in the subsequent ddPCR reaction. For the analysis of the ES metastatic model, 4-plex ddPCR assays (Figure S1) were performed on organ-derived gDNAs (approximately 200 ng or 400 ng of liver- or lung-derived gDNA, respectively) to simultaneously detect the presence of all different cell types (TC71 Luc tumour cells, gene-

modified MSCs, and murine cells). The control 4-plex ddPCR assay (Figure S1a) combined Luc (270 nM primers/75 nM probe) and GFP (1 125 nM primers/312.5 nM probe) target assays with mTfrc and hRPP30 reference assays (both at 900 nM primers/250 nM probe), which allowed for the detection of murine cells and human cells localised in mouse organs, represented by TC71 Luc tumour cells and EV or GD2 tCAR control MSCs. In the sTRAIL 4-plex ddPCR assay (Figure S1b), Luc (765 nM primers/212.5 nM probe) and sTRAIL (900 nM primers/250 nM probe) target assays were combined with the mTfrc (765 nM primers/212.5 nM probe) and hRPP30 (900 nM primers/250 nM probe) reference assays to simultaneously detect murine cells and human cells, allowing for the distinction between TC71 Luc tumour cells and sTRAIL or BF effector MSCs. The target and reference gene concentrations were divided by the respective gene CNs to calculate the numbers of TC71 Luc cells and gene-modified MSCs and the numbers of human and murine cells per µl of the ddPCR reaction. The total number of cells per µl was obtained by combining the human and murine cell numbers. Ratios between the number of TC71 Luc cells (or gene-modified MSCs) per µl and the total number of cells per µl were calculated. For each mouse group, the median (IQR) values were derived and multiplied by 1 000, and the groups were then compared in terms of metastases growth and MSC distribution. Ratios between the numbers of gene-modified MSCs and TC71 Luc tumour cells in both the lungs and liver were also obtained for each group.

Histology

Formalin-fixed, paraffin-embedded lung and liver sections were evaluated by haematoxylin (Bio Optica, Milan, Italy) and eosin (Sigma-Aldrich) staining (H&E). Sections were examined using a Zeiss Axio-Scope microscope (Zeiss, Oberkochen, Germany). Photomicrographs were acquired using an AxioCam ICc3 colour camera and AxioVision software (Zeiss).

Ethics

All animal studies were conducted in accordance with the institutional and national guidelines and under approved protocols by the Local Ethical Committee on Animal Experimentation and by the Italian Ministry of Health (authorisation no: 22/2020 PR).

Statistics

In vitro data are expressed as the mean ± standard deviation (SD). A two-tailed p-value of $< .05$, assessed using Student's t-test, was considered significant. Each experimental group was assayed at least twice in triplicate. Analyses were performed using Excel 2020 (Microsoft Inc., Redmond, WA, USA). In vivo data were reported as the median and IQR. Comparisons between different experimental groups were performed by using the Wilcoxon-Mann-Whitney test, whereas comparisons between the lungs and liver or between time points within the same experimental group were performed using the Wilcoxon signed-rank test for paired data. The analyses were performed with R, 3.4.3, statistical software (The R Foundation for Statistical Computing, Wien, Austria). All tests were two-tailed, and the confidence level was 95% ($p < .05$).

Role of funding source

The funding sources played no role in the study design, data collection, data analysis, interpretation, writing of the report, and the decision of paper submission.

Results

BF MSCs express GD2 tCAR and secrete TRAIL

The co-expression of GD2 tCAR and sTRAIL in MSCs was achieved through lentiviral vector transduction. The presence of sTRAIL and GD2 tCAR molecules in transduced MSCs was verified by FACS (Fig. 1b). TRAIL and GD2 tCAR were undetectable in EV MSCs (Fig. 1b, first row), whereas GD2 tCAR was exclusively detected in 79.1% ± 7.0% of GD2 tCAR MSCs (Fig. 1b, second row), as previously reported [37]. The expression of TRAIL was confirmed for 99.9% ± 0.6% of sTRAIL-transduced MSCs (24.1% ± 8.5% on the cell membrane and 75.8% ± 8.9% in the cytoplasm; Fig. 1b, third row). BF MSCs expressed sTRAIL together with GD2 tCAR. TRAIL expression was detected in 89.3% ± 13.4% of BF MSCs (15.0% ± 5.2% on the cell membrane and 74.6% ± 17.5% in the cytoplasm), and 85% ± 17% of BF MSCs were also positive for GD2 tCAR (Fig. 1b, fourth row). Gene-modified MSCs were further tested for sTRAIL secretion (data not shown). ELISA confirmed that different batches ($n = 2$) of sTRAIL MSCs were capable of releasing an average of 782.3 ± 131.6 pg/ml of sTRAIL. The secretion of sTRAIL by BF MSCs ($n = 2$) was also confirmed by ELISA, obtaining an average of 783.4 ± 415.9 pg/ml of sTRAIL. EV and GD2 tCAR MSCs did not spontaneously release sTRAIL. These findings demonstrated that the high levels of GD2 tCAR expression on BF MSCs does not affect sTRAIL production, indicating the feasibility of our dual-targeting approach.

GD2 tCAR mediates strong interactions between BF MSCs and GD2-expressing ES cells

After generating the effector cells, we began testing the GD2 on three different ES cell lines, as predictive factor for affinity-based targeting. FACS analyses revealed that the three selected ES cell lines expressed different levels of GD2 (Figure S2). Specifically, we were able to distinguish ES cell lines in the GD2-higly positive TC71 (99.7% ± 0.1%), the weakly GD2-positive A673 (17% ± 10%) and the GD2-negative RD-ES (1.5% ± 1%).

MSC surface functionalisation with GD2 tCAR was able to force an interaction between BF MSCs expressing mTRAIL and GD2-positive GBM cells [37]. Here, BF MSCs that release sTRAIL and simultaneously express GD2 tCAR were tested for their ability to bind GD2-positive ES cells in a cell-to-cell interaction assay (Fig. 2), as previously described [37]. Briefly, DsRed-expressing ES cells were added to CFSE-labelled MSC monolayers and allowed to interact for 1.5 h. Cells were analysed by FACS to determine the absolute numbers of MSC-ES cell aggregates, visualised as CFSE/DsRed double-positive events. The numbers of aggregates were normalised against the number of aggregates formed by EV MSC-ES cell interactions, and the data were presented as the fold change. The aggregates formed by BF MSCs bound to the highly GD2-positive TC71 line were at least three-fold as many as those formed by EV MSCs and sTRAIL MSCs ($p < .001$; Fig. 2a), which was similar to the number of aggregates formed by GD2 tCAR MSCs ($p > .05$). A lower interaction rate for BF MSCs was observed in the weakly GD2-positive A673 line, although the binding was still appreciable compared with EV MSCs ($p < .05$; Fig. 2b). For the GD2-negative RD-ES line, no differences in aggregate formation were detected between the MSC groups (Fig. 2c). The role played by GD2 tCAR in strengthening the binding between cells was further confirmed by examining EV and GD2 tCAR MSC interactions with TC71 cells (Fig. 2d). After the initial detachment (T0), MSC-TC71 cell aggregates were maintained in non-permissive conditions at 4 °C on a rotating support for 2 and 4 h. After 2 h, the binding capacity of GD2 tCAR MSCs did not significantly decreased relative to that at baseline (T0), whereas EV MSC binding reduced ($p < .001$). After 4 h, the GD2 tCAR MSC-ES aggregate number remained stable, whereas EV MSC-ES aggregates decreased in number compared with both the 2 h and T0 time points ($p < .05$). Overall, BF MSCs showed enhanced binding with ES cells expressing GD2 as the

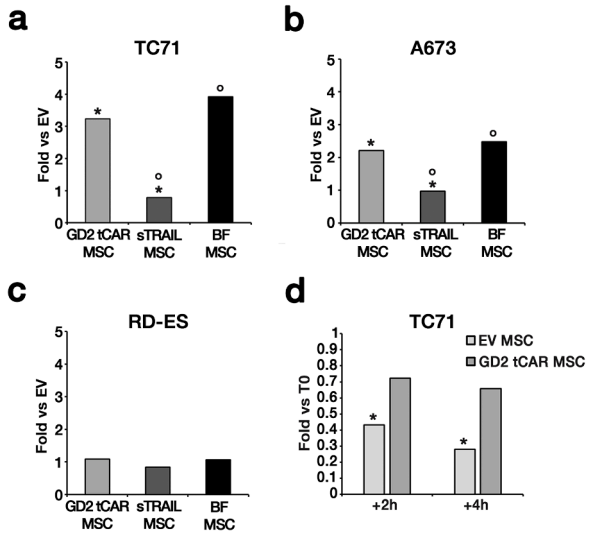

Fig. 2. BF MSCs establish strong and stable connections with GD2-expressing ES cells. GD2 tCAR-mediated binding of MSCs to ES cell lines was investigated using cell-to-cell interaction assays. **a-c**, The number of MSC-ES cell aggregates, reported as the fold change versus EV MSCs, for all three ES cell lines. For TC71 $*p < .001$, $°p < .001$; for A673 $*p < .05$, $°p < .001$. **d**, The stability of the GD2 tCAR-mediated binding was examined by comparing the interactions of EV and GD2 tCAR MSCs with the TC71 ES line. MSC-TC71 aggregates were maintained at 4 °C on a rotating support for 2 and 4 h, and the number of aggregates was quantified by FACS. The number of MSC-TC71 aggregates at 2 and 4 h is reported as the fold change relative to the respective baseline number at the time of detachment (T0). $*p < .05$. All-p values were calculated by Student's *t*-test. Data are expressed as the mean (SD). Numbers of independent experiments $n = 2$, each with three technical replicates.

result of specific and stable cell-to-cell interactions mediated by GD2 tCAR on the MSC surface. The co-expression of sTRAIL in BF MSCs did not affect the GD2 tCAR-mediated binding enhancement, supporting the evaluation of our affinity-based anticancer strategy in GD2-positive ES.

BF MSCs or their supernatants display potent antitumour activities against ES cells in vitro

First, we examined TRAIL receptor expression on the three ES cell lines, as predictive factor for TRAIL sensitivity (Figure S3a). FACS analyses revealed high levels of DR5 (≥95%) and low levels of DR4 expression (≤25%) in all cell lines. The decoy receptor DcR1 was undetectable in all cell lines (<4%), whereas DcR2 was highly expressed in TC71 cells (85.8% ± 7.7%), with a low level of expression in A673 cells (20.9% ± 8.5%) and negative in RD-ES cells (1.8% ± 0.4%). Dose-response tests were performed to confirm the rhTRAIL sensitivity of ES cell lines (Figure S3b). Despite similarly high expression levels of DR5, the ES lines responded differently to rhTRAIL, with the A673 and RD-ES cell lines being the most sensitive (23.5% ± 0.7% and 11.4% ± 3.1% cell viability, respectively; $p < .001$), whereas TC71 cells had the lowest sensitivity (57.5% ± 1.1% cell viability; $p < .05$) after incubation for 24 h with the highest rhTRAIL dose (1 μg/ml). These data suggested that the considered ES cell lines could be suitable targets for TRAIL-mediated apoptosis.

Co-cultures were performed to verify the effectiveness of our strategy based on BF MSCs expressing sTRAIL and GD2 tCAR. The killing mediated by BF MSCs, which was tested at multiple T:E ratios (1:1; 1:2, and 1:5; Fig. 3a-c), was assessed after 24 h of co-culture. In all conditions, the culture media were pre-conditioned overnight by MSCs or rhTRAIL before adding the ES target cells. All tested ES cell lines displayed a strong sensitivity to BF MSCs. BF MSCs were able to induce a potent cytotoxic effect, even at the lowest 1:1 ratio, with levels that remained stable regardless of the effector number. A673 was observed to be the most sensitive line, with up to 92.7% ± 1.2% cell death at the 1:2 ratio (Fig. 3b). At a 1:2 ratio BF MSCs were also able to exert robust cytotoxic effects against TC71 and RD-ES cells (88.4% ± 3.6% and 88.6% ± 4.3% respectively, $p < .001$; Fig. 3a and c) provoking a mortality rate comparable to that observed for sTRAIL MSCs ($p > .05$) and superior to that induced by rhTRAIL (1 μg/ml) in the TC71 line ($p < .001$). For all ES lines, the co-culture with EV MSCs or GD2 tCAR MSCs had no impact on tumour cell viability.

To assess the cytotoxicity of the sTRAIL released by MSCs (Fig. 3d-f), tumour cells were incubated for 24 h with SNs collected from sTRAIL and BF MSCs. SNs from sTRAIL and BF MSCs induced significant levels of cell death against all ES lines compared with those for the CTR, EV, and GD2 tCAR MSC control groups. The A673 line (Fig. 3e) again showed the highest sensitivity to sTRAIL, reaching up to 71.1% ± 10.3% cell death following incubation with BF MSC SN, which was similar to levels observed for rhTRAIL (1 μg/ml, $p > .05$). Of notice, the BF MSC sTRAIL mean concentration was approximately 4000-fold less (253.5 ± 10 pg/ml) than the concentration of rhTRAIL. BF MSC SN induced 58.5% ± 18.9% and 59.1% ± 5.8% cell death in the TC71 and RD-ES cell lines, respectively (Fig. 3d and f), similarly to the levels observed in response to SN from sTRAIL MSC ($p > .05$). Together these in vitro data indicate the significant sensitivity of ES cells towards sTRAIL delivered by MSCs. We demonstrated that the simultaneous release of sTRAIL and the expression of GD2 tCAR did not affect the killing by engineered MSCs, further encouraging our dual-targeting approach against GD2-positive ES.

BF MSCs induce apoptosis in TC71 and A673 cell lines in spheroid co-cultures

The cytotoxicity by BF MSCs was further explored in 3D in vitro settings. Tumour spheroids were established using TC71 and A673 cell lines. After 24 h, spheroids were treated with either rhTRAIL or gene-modified MSCs (Fig. 4). Representative images for the TC71 cell line are shown in Figures S1 and 5a. The cells were first tested for their ability to form spheroids (Figure S4, CTR, first row), which indicated that TC71 spheroid formation was a bi-phasic process of aggregation due to cellular rearrangements, resulting in moderate compaction within 24 h. Subsequently, the TC71 spheroid was challenged with rhTRAIL (1 μg/ml) to examine whether the 3D conformation would confer resistance to the proapoptotic signal of the ligand. As observed in Figure S4 (rhTRAIL, second row), rhTRAIL treatment provoked TC71 cell death, strongly disrupting the 3D architecture and reducing both fluorescence intensity and spheroid size. In co-culture, at 8 h, MSCs progressively gathered around the tumour spheroid (Fig. 4a, 8 h, first column), and after 24 h, MSCs began to interact with tumour cells provoking the apparent shrinkage of the red spheroid (Fig. 4a, 24 h, second column). The differences associated with different MSC gene modifications became clear at 48 h (Fig. 4a, 48 h, third and fourth columns): both EV and GD2 tCAR MSC green fluorescence appeared to concentrate at the centre of the spheroid, interspersed with the red tumour cells. When examining frozen sections taken at deep levels by cryostat serial cutting (Fig. 4a, 48 h, frozen sections), control MSCs greatly intruded into the red TC71 spheroid, reaching the core (Fig. 4a, 48 h, frozen sections, EV and GD2 tCAR MSCs). By contrast, sTRAIL and BF MSCs progressively destroyed the red sphere, and DsRed fluorescence slightly faded due to cellular damage; frozen sections highlight the complete loss of the spheroid architecture as a result of the disruption of cell-to-cell interactions caused by TRAIL-mediated cell death (Fig. 4a, 48 h, frozen sections, sTRAIL and BF MSCs). In particular, the DsRed-labelled TC71 cells are almost completely lost in the frozen sections of spheroid co-cultured with BF MSCs. A time point of 15 h was identified as the optimal timing to quantify the effect of BF MSCs in terms of both reduced tumour cell viability and caspase-8 activation (Fig. 4b-e). For TC71, cell viability was lower in spheroids co-cultured with sTRAIL and BF MSCs compared

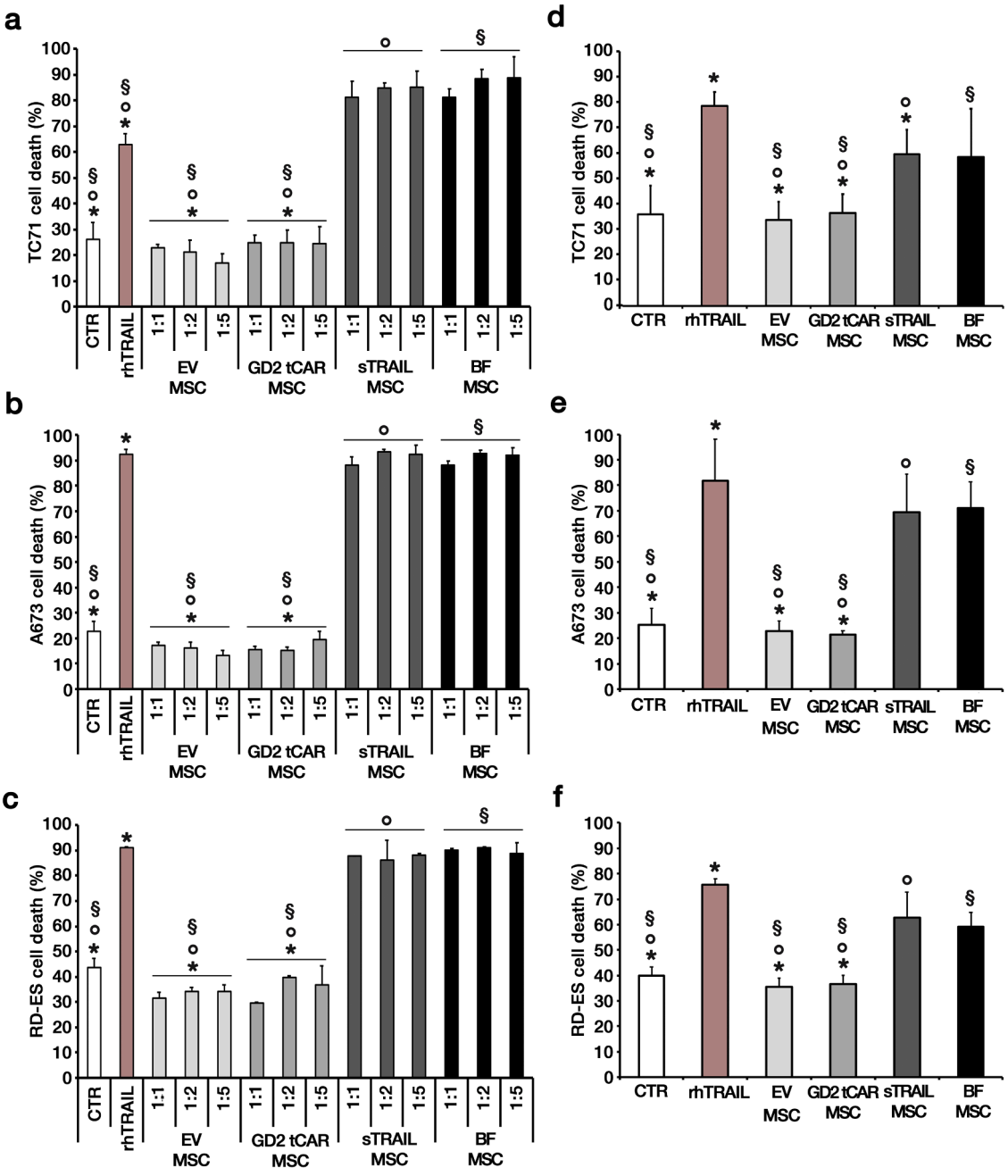

Fig. 3. BF MSCs and their conditioned supernatants exert in vitro cytotoxic effects against targeted ES cell lines. The in vitro impact of BF MSCs against the ES cell lines **a**, TC71 **b**, A673 and **c**, RD-ES was examined by co-cultures using multiple target:effector ratios (1:1; 1:2, and 1:5). Recombinant human TRAIL (rhTRAIL, 1 μg/ml) was used as a positive control, whereas tumour cells cultured alone were used as the negative control (CTR). Tumour cell death was examined by supravital propidium iodide (PI) after 24 h. Reported p-values represent the results of multiple comparisons between sTRAIL and BF MSC conditions and control groups, represented by EV MSCs, GD2 tCAR MSCs, rhTRAIL, or CTR. For TC71 $^{*}p < .001$, $^{\circ}p < .01$, $^{\S}p < .01$; for A172 $^{*}p < .001$, $^{\circ}p < .001$, $^{\S}p < .001$; for RD-ES $^{*}p < .001$, $^{\circ}p < .001$, $^{\S}p < .001$. sTRAIL-mediated cytotoxicity against **d**, TC71 **e**, A673 and **f**, RD-ES cell lines. Tumour cells were incubated for 24 h with sTRAIL-containing supernatants (SNs) collected from sTRAIL and BF MSCs. SNs deriving from EV and GD2 tCAR MSCs were used as controls. ES cells in normal culture media (CTR) or treated with rhTRAIL (1 μg/ml) were evaluated for comparison. After 24 h, tumour cell death was assessed by supravital PI. For TC71 $^{*}p < .05$, $^{\circ}p < .001$, $^{\S}p < .05$; for A673 $^{*}p < .001$, $^{\circ}p < .001$, $^{\S}p < .001$; for RD-ES $^{*}p < .01$, $^{\circ}p < .001$, $^{\S}p < .001$. All-p values have been calculated by Student's *t*-test. Data are expressed as the mean (SD). Numbers of independent experiments $n = 2$, each with three technical replicates.

with those in co-culture with EV and GD2 tCAR MSCs ($p < .001$; Fig. 4b). In parallel, BF MSCs were able to strongly activate caspase-8 in TC71 spheroids compared with EV and GD2 tCAR MSCs ($p < .001$; Fig. 4c), which was also observed for sTRAIL MSCs, and this activation appeared to be higher than that mediated by rhTRAIL, although without achieving significance ($p > .05$). No caspase-8 activation was observed for either EV or GD2 tCAR MSCs. Similar findings were obtained for A673 spheroids (Fig. 4d and e). These assays indicated that BF and sTRAIL MSCs displayed similar cytotoxic effects, even in the 3D setting, confirming that the presence of GD2 tCAR does not affect the killing capacity of BF MSCs.

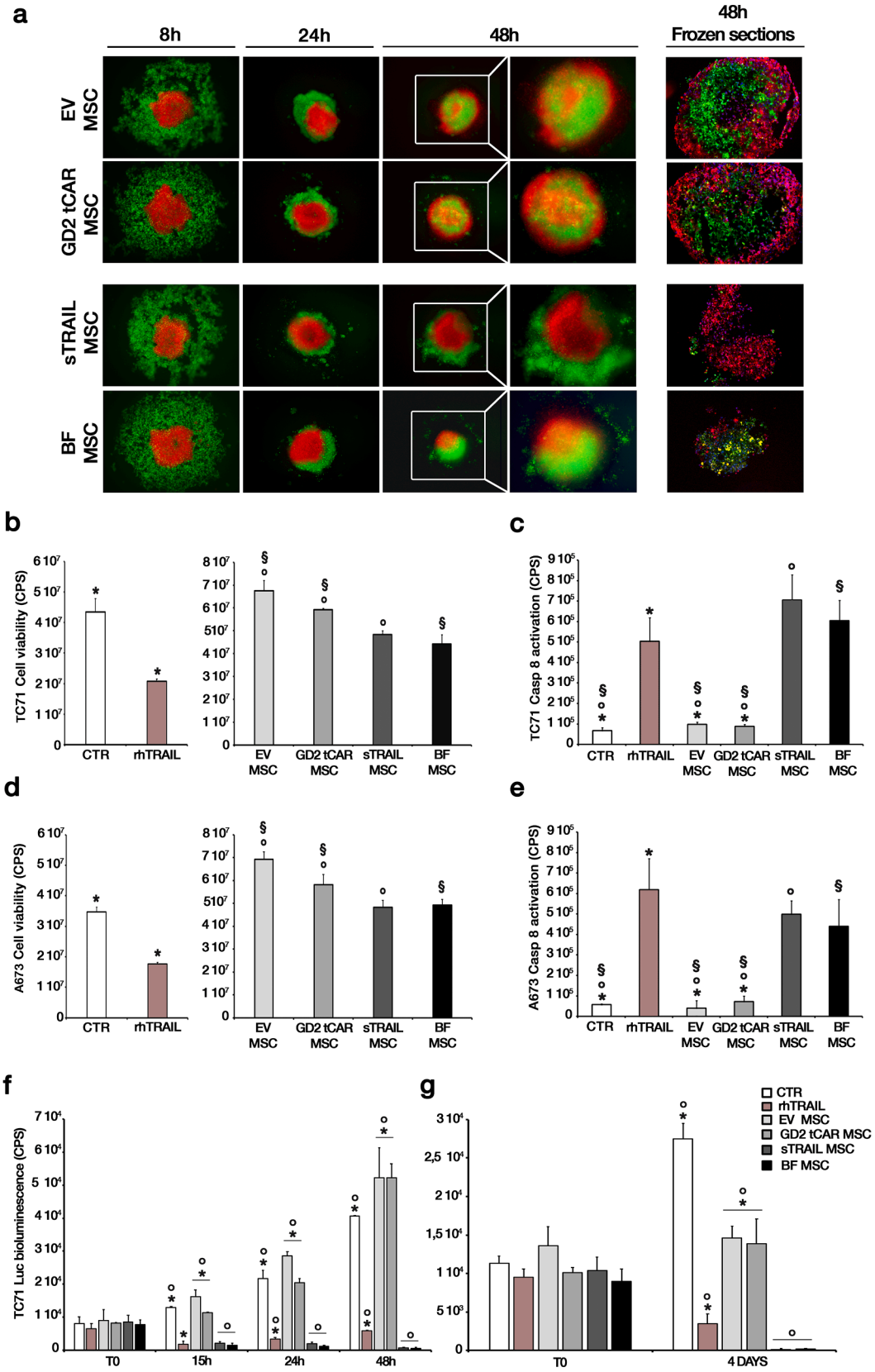

(caption on next page)

Fig. 4. BF MSCs display potent antitumour activities against ES spheroid models. **a**, Tumour spheroids were established using DsRed-expressing TC71 and A673 cells (red) and treated with MSCs labelled with CFSE (green). Tumour spheroids were monitored for MSC infiltration and cytotoxicity for up to 48 h of co-culture by fluorescence microscopy and frozen sections at deep levels obtained by cryostat serial cutting. Representative images of the TC71 cell line are shown (magnification 50x, columns 1–3, and 100x, columns 4 and 5). The 15-hour time point was identified as the optimal time to quantify the antitumour effects of BF MSCs on TC71 and A673 spheroids, in terms of both reduced cell viability (**b** and **d**) and caspase-8 activation (**c** and **e**) by luminescence-based assays. For cell viability assay, TC71 $^{*}p < .001$, $^{\circ}p < .01$, $^{\S}p < .01$; A673 $^{*}p < .001$, $^{\circ}p < .01$, $^{\S}p < .01$. For caspase-8 activation assay TC71 $^{*}p < .01$, $^{\circ}p < .001$, $^{\S}p < .001$; A673 $^{*}p < .01$, $^{\circ}p < .001$, $^{\S}p < .001$. **f** and **g**, A 3D fibre-based matrix was employed to better model the tumour architecture. Bioluminescent signal after luciferin administration was used to quantify the viability of TC71 cells seeded on the matrix. The killing capacity of BF MSCs in co-culture with TC71 Luc (T:E ratio of 3:1) was assessed in a time-course experiment (**f**, $^{*}p < .01$, $^{\circ}p < .05$) and an endpoint assay after 4 days (**g**, $^{*}p < .01$, $^{\circ}p < .01$). The BF MSC cytotoxic effect was compared to those of rhTRAIL alone (1 μg/ml) and MSCs expressing sTRAIL only. EV MSCs, GD2 tCAR MSCs, and TC71 cells alone (CTR) were used as negative controls. The basal bioluminescence of the 3D matrix loaded by TC71 Luc cells was assessed immediately before MSC seeding or rhTRAIL treatment (T0). All p-values were calculated by Student's *t*-test. Data are expressed as the mean (SD). Numbers of independent experiments $n = 2$, each with three technical replicates.

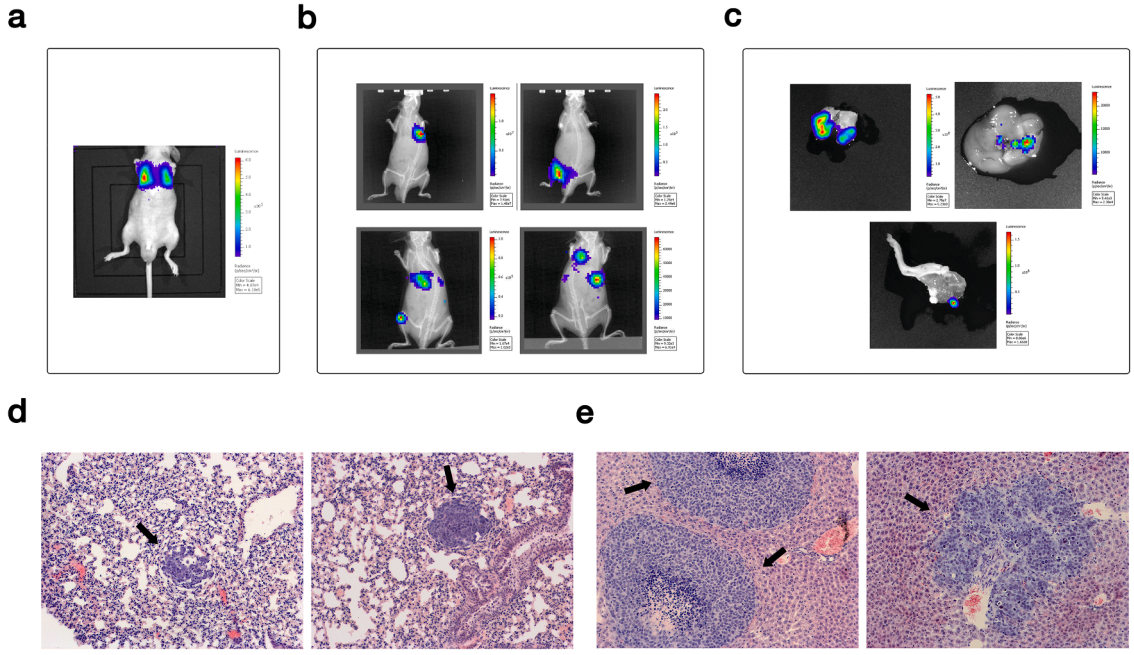

Fig. 5. Establishment of an in vivo model that closely mimics metastatic ES. Two million TC71 Luc cells were intravenously injected into NSG mice. TC71 Luc cell engraftment was assessed by monitoring in vivo bioluminescence using the IVIS system. **a**, Ten minutes after TC71 Luc cell injection, the luminescence signal accumulated in the lung. **b**, Over the next few hours, the bioluminescence gradually disappeared as the cells dispersed and re-emerged 10 days later at various locations where tumours developed. The most common engraftment sites were the lungs, liver, and femur. **c**, At sacrifice, on day 13, metastases were quantified in extracted organs by IVIS. **d** and **e**, Tumour metastases (black arrows) were confirmed by H&E staining on lung (**d**) and liver (**e**) sections (magnification 100x).

BF MSCs can target a 3D matrix model of ES

In a miniaturised 3D system, such as a spheroid, the self-assembly of cells in large aggregates creates zones that are not equally exposed to nutrients, gas, and waste, which can affect the proper modelling of the tissue of interest [41]. We employed a polyester-based 3D matrix to recreate a tumour structure to bridge our in vitro and in vivo studies. This 3D matrix has recently been employed to form the 3D inner core of the VITVO™ (Rigenerand Srl, Medolla, Modena, Italy) [41]. TC71 cells have been engineered to express a red-shifted *Luciola italica* luciferase transgene, and the obtained TC71 Luc cells were tested by IVIS, resulting in a photon emission of 1 774 ± 582 photons/second (p/s) per cell (data not shown). The bioluminescent signal after luciferin administration was used to quantify tumour cell viability on the matrix, with high sensitivity (Fig. 4f and g). Once seeded, TC71 Luc cells attached to the matrix fibres, migrated, and proliferated into the matrix (Fig. 4f and g, white columns). After 12 h, the basal bioluminescence of the matrices was collected before MSC seeding or rhTRAIL (1 μg/ml) treatment and appeared to be homogenous ($p > .05$; Fig. 4f and g, T0). After 15 h of co-culture, BF MSCs strongly reduced TC71 Luc cell viability, with similar effects observed for sTRAIL MSCs and rhTRAIL treatment (Fig. 4f). However, after 24 and 48 h of co-culture, both BF and sTRAIL MSCs were more effective for killing tumour cells and controlling tumour growth than rhTRAIL treatment ($p < .05$ and $p < .01$, respectively; Fig. 4f). This increase in effectivity was clearly visible at the longer time point of 4 days ($p < .01$ for both; Fig. 4g), indicating the advantage of using MSCs that constantly release sTRAIL over the administration of rhTRAIL. In the time-course experiment, co-cultures of TC71 Luc matrices with EV or GD2 tCAR MSCs did not impact tumour cell survival (Fig. 4f). After 4 days, TC71 Luc cell viability in co-cultures with both EV and GD2 tCAR MSCs was lower than that of the CTR culture ($p < .05$; Fig. 4g), which may be caused by culture media exhaustion. Collectively, we confirmed that BF MSCs could effectively induce both short- and long-term cytotoxicity against ES cells that have been grown under conditions that facilitated their reorganisation into a 3D tumour structure.

Establishment of a reliable and reproducible in vivo model of ES metastases

Before introducing the therapeutic protocol, we established few in vivo ES models aiming to stably recreate the metastatic disease and then investigate whether the inclusion of GD2 tCAR could specifically improve the tumour-targeting and killing functions of BF MSCs. We employed NSG mice, one of the most immunodeficient mouse strains

that have been described, to date, in which the only effective immune cells in the peripheral blood are neutrophils and monocytes [42]. In a pilot study, NSG mice ($n = 24$) were i.v. inoculated with two million TC71 Luc cells. The direct introduction of tumour cells into the bloodstream recapitulates the colonisation phases of metastases, a process that consists of cellular arrest, extravasation, and proliferation [43]. The pattern of TC71 Luc cell engraftment (Fig. 5) was assessed by acquiring serial images of in vivo bioluminescence until the mice were sacrificed. Ten min after tumour cell i.v. injection, the luminescence signal was found in the lung area, indicating the entrapment of TC71 Luc cells within the capillary bed of the lung (Fig. 5a). In this model, 100% of mice developed clear metastases as early as 10 days after TC71 Luc injection, as assessed by IVIS (Fig. 5b). The engraftment sites include the lungs, liver, femur, mandible, and pelvis, which are similar to the most frequently observed metastases sites in ES patients [44]. Metastases in the mandible and pelvis were rare, affecting only 28.6% and 19.0% of mice, respectively, by day 16. At the time of sacrifice, day 17, metastases were confirmed at the most common sites by assessing the bioluminescence of the extracted organs using IVIS (Fig. 5c), which revealed lung metastases in 90.5% of mice, liver metastases in 90.5% mice, and femur metastases in 57.1% mice. As a measure of tumour cell viability, the average bioluminescent signals observed for the lung and liver metastases were similar ($1.4 \times 10^7 \pm 3.1 \times 10^7$ p/s and $1.2 \times 10^7 \pm 1.0 \times 10^7$ p/s, respectively, $p > .05$; data not shown), whereas lower signals were measured for the femur nodules ($2.8 \times 10^5 \pm 2.7 \times 10^5$ p/s, $p < .05$ versus liver; data not shown). The H&E staining of lung tissue sections (Fig. 5d) confirmed the presence of small tumour masses composed of round cells with hyperchromatic nuclei and little basophilic cytoplasm. In tissue sections from the liver (Fig. 5e), we found large tumour masses with central necrotic areas, explaining the lower-than-expected viability assessed by the bioluminescence analysis. At day 15, the mice were i.v. injected with one million of DiR-labelled EV or GD2 tCAR MSCs to further investigate the MSC distribution in vivo. The MSC distribution was followed by IVIS, which showed that MSCs appeared to localise primarily in the lungs and liver (data not shown). The presence of MSCs in dissociated lungs ($n = 12$) was evaluated by FACS (Figure S5a and b), reporting a 0,6 ± 0.4% of MSCs (data not shown). MSCs were also detected on lung sections by the GFP staining (Figure S5c). Expression of GD2 by tumour metastases was confirmed by FACS analysis on freshly isolated cells from lungs and livers of tumour-bearing mice ($n = 3$; Figure S6). GD2 expression was observed on all tumour cells co-labelled with CD105, a marker highly expressed by TC71 cells (data not shown). Overall, the NSG was found to be the best strain for reproducing the complexity of severe metastatic disease, in which multiple sites are affected by metastatic growth.

BF MSCs are able to reduce lung metastases in the ES metastatic model

To further strengthen the rationale of our cell-based approach, we then explored the BF MSC antitumour potential using the generated NSG metastatic model of ES. EV and GD2 tCAR control MSCs were additionally modified to express GFP and were sorted (93.9% ± 0.4% GFP^+ and 95.9% ± 0.4% GD2 $tCAR^+/GFP^+$, respectively; data not shown) to detect their presence in mouse tissues by ddPCR.

TC71 Luc cells were i.v. injected into NSG mice, and engraftment was tracked using in vivo bioluminescence. Starting on day 4 after TC71 Luc cell injection, we treated the mice with three doses of gene-modified MSCs, once every three days (Fig. 6a). Unfortunately, three mice were lost at various times during this experiment due to pulmonary embolism after the MSC infusions. Clear metastases were identified in 100% of CTR mice at 12 days after tumour cell injection by IVIS. Metastases in the femur, mandible, and pelvis were rare, affecting 22.7%, 18.2%, and 9.1% of mice, respectively. At the time of sacrifice, on day 13, bioluminescence was quantified in the lungs and liver, which represented the primary organs affected by tumour growth, with lung metastases detected in 86.4% of mice and liver metastases detected in 90.9% of mice. The bioluminescent signals strongly differed between lung and liver metastases (data not shown). Because of the earlier time point sacrifice, 15/19 (78.9%) of lungs affected by metastases displayed signals under the noise level (<600 counts), preventing correct quantification by IVIS. By contrast, all of the signals derived from liver metastases were above the background level, with an average total flux of $5.3 \times 10^6 \pm 6.4 \times 10^6$ p/s. Due to the inadequate sensitivity of optical imaging, we set up a ddPCR-based technique to accurately quantify the response to BF MSC therapy. After sacrifice, lung- and liver-derived gDNA were analysed for the presence of specific tumour DNA using the control and sTRAIL 4-plex ddPCR assays described in material and methods. The results are presented as lung and liver box plots using a logarithmic scale (Fig. 6b and c). The tumour cell quantity in the liver was significantly higher than that in the lungs for all groups ($p < .005$).

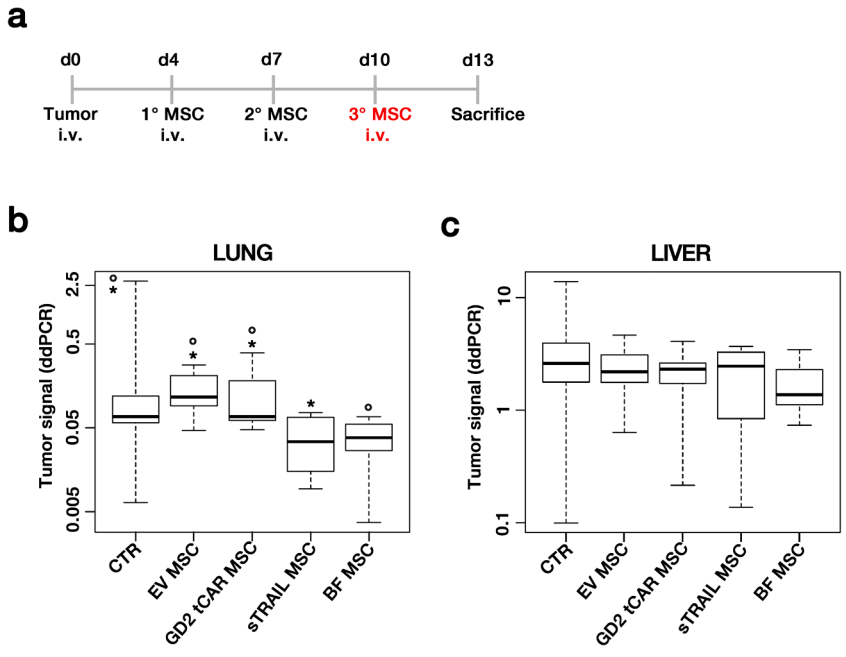

Fig. 6. BF MSCs are able to reduce lung metastases in the ES metastatic model. The BF MSC antitumour potential was examined in a metastatic model of ES. **a**, Representative therapeutic schedule: TC71 Luc cells (two million) were intravenously (i.v.) injected into NSG mice ($n = 62$). Starting four days after TC71 Luc cell injection, the animals were randomly divided into five groups for treatment: control group ($n = 22$) received no treatment (CTR); the EV MSC group ($n = 10$), GD2 tCAR MSC group ($n = 10$), sTRAIL MSC group ($n = 10$), and BF MSC group ($n = 10$) received multiple ($n = 3$) i.v. injections of one million of the respective gene-modified MSCs, which were administered every three days. Before the infusion, the third dose of gene-modified MSCs was labelled by DiR dye (8 μM; in red). After 13 days, the animals were sacrificed. Lungs and liver were extracted, maintained on dry ice, and stored at −80 °C. 4-plex ddPCR assays were performed on organ-derived gDNA to simultaneously detect the presence of various cell types. **b** and **c**, Ratios of TC71 Luc cells per μl to the total number of cells per μl were calculated for lungs and liver. For each mouse group, the median (interquartile range; IQR) values were derived and multiplied by 1000, and groups were compared in terms of metastatic growth in lungs (**b**) and liver (**c**). For the lungs, sTRAIL MSCs vs CTR, EV MSCs or GD2 tCAR MSCs $*p < .05$, BF MSCs vs CTR, EV MSCs or GD2 tCAR MSCs $°p < .05$. All p-values were calculated by the Wilcoxon–Mann–Whitney test.

We observed a marked decrease in the tumour burden identified in the lungs of mice receiving BF MSC therapy compared with the CTR [0.038 (0.021 to 0.058) vs 0.068 (0.0554 to 0.1217), 0.6-fold change; $p < .05$], EV MSC [0.038 (0.021 to 0.058) vs 0.117 (0.087 to 0.243), 0.3-fold change; $p < .0001$], and GD2 tCAR MSC [0.038 (0.021 to 0.058) vs 0.068 (0.057 to 0.212), 0.6-fold change; $p < .01$] control groups (Fig. 6b). The sTRAIL MSC antitumour effect in the lungs was similar to that observed for BF MSCs [0.034 (0.014 to 0.069) vs 0.038 (0.021 to 0.058), 1.1-fold change; $p > .05$], resulting in a significant decrease in lung metastases when compared with the CTR [0.034 (0.014 to 0.069) vs 0.061 (0.040 to 0.084), 0.6-fold change; $p < .05$], EV MSC [0.034 (0.014 to 0.069) vs 0.117 (0.087 to 0.243), 0.3-fold change; $p < .001$], and GD2 tCAR MSC [0.034 (0.014 to 0.069) vs 0.068 (0.057 to 0.212), 0.5-fold change; $p < .05$] control groups (Fig. 6b). When examining the liver, we observed a modest antitumour effect in the BF MSC group, which failed to achieve significance compared with the CTR [1.375 (1.037 to 2.561) vs 2.610 (1.751 to 4.075), 0.5-fold change; close to borderline significance ($p = .070$)], EV MSC [1.375 (1.037 to 2.561) vs 2.915 (1.276 to 3.633), 0.6-fold change; $p > .05$], or GD2 tCAR MSC [1.375 (1.037 to 2.561) vs 2.318 (1.182 to 3.202), 0.6-fold change; $p > .05$] groups (Fig. 6c). The sTRAIL MSC did not show a significant antitumour effect on liver metastases compared with the CTR [2.461 (0.797 to 3.318) vs 2.610 (1.751 to 4.075), 0.9-fold change; $p > .05$], EV MSC [2.461 (0.797 to 3.318) vs 2.915 (1.276 to 3.633), 1.1-fold change; $p >$

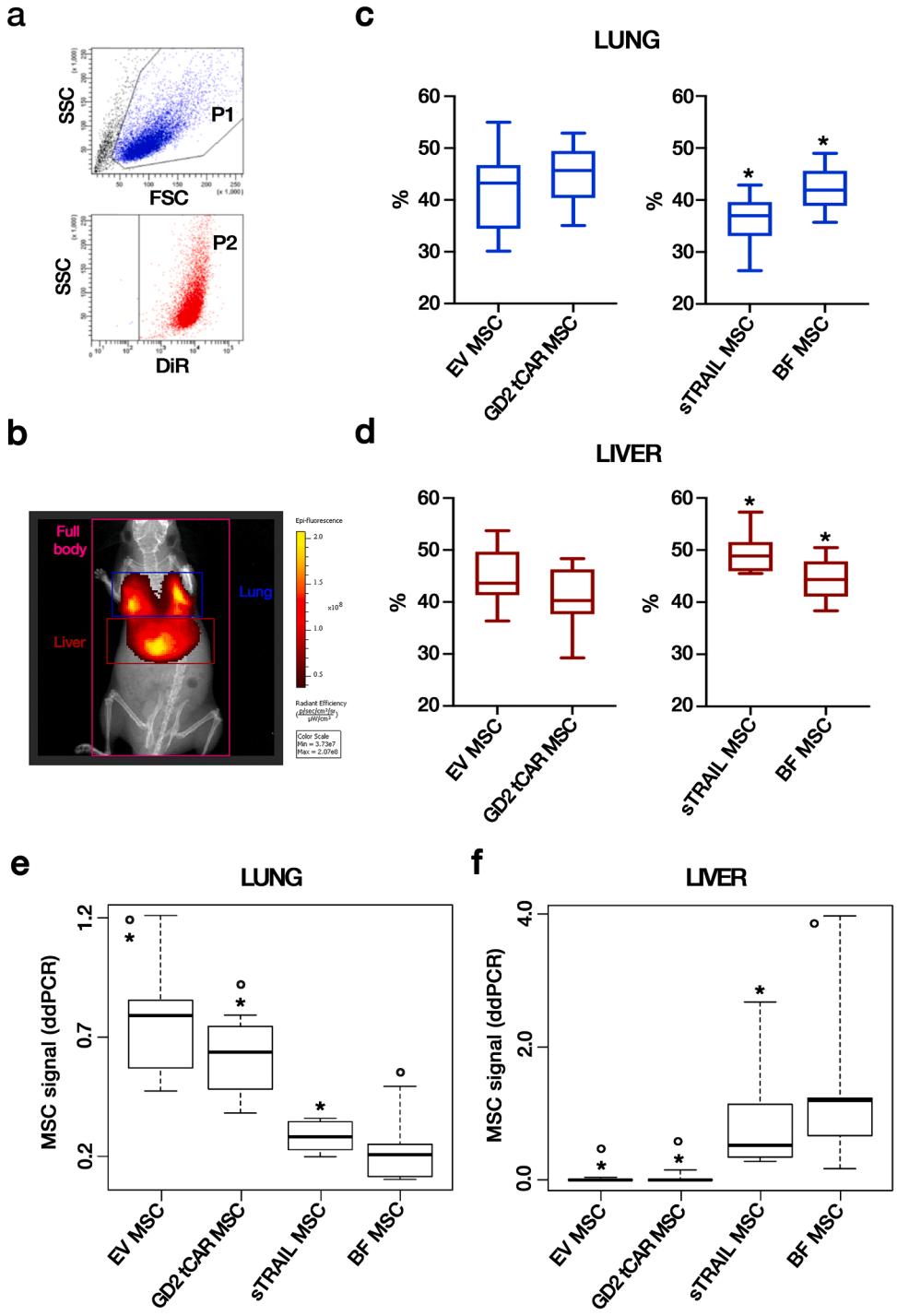

Fig. 7. GD2 tCAR strengthens the binding of BF MSCs to ES metastases, early in the lungs and later in the liver. The final dose of gene-modified MSCs was labelled by DiR dye (8 μM) before the infusion to investigate the MSC biodistribution and tumour-targeting efficiency. **a**, The DiR labelling strategy was validated in vitro and confirmed by FACS analysis. Cells were first gated on forward scatter area (FSC) and side scatter area (SSC) to exclude debris (P1), then DiR-labelled MSC (P2) populations were identified. **b,** DiR-labelled MSCs were followed for two days after intravenous administration by IVIS. Data were collected by applying fixed ROIs to the lungs and liver, which are the primary organs affected by tumour growth and in which DiR fluorescence localised over time. **c** and **d**, DiR signals in the organs were normalised to full body DiR fluorescence. The ratios for the lungs (**c**) or liver (**d**) were expressed as a percentage and median (interquartile range; IQR) values were calculated. Box plots show the data for an early time point of 4 h after MSC infusion. For the lungs, $*p < .05$. For the liver, $*p < .05$. **e** and **f**, Three days after MSC infusion, MSC engraftment was confirmed on extracted organs by control or sTRAIL 4-plex ddPCR assays. Ratios of the number of gene-modified MSCs per μl to the total number of cells per μl were calculated. For each mouse group, the median (IQR) values were derived and multiplied by 1000, and groups were then compared in terms of MSC distribution in lungs (**e**) and liver (**f**). For the lungs, sTRAIL MSCs vs CTR, EV MSCs or GD2 tCAR MSCs $*p < .001$, BF MSCs vs CTR, EV MSCs or GD2 tCAR MSCs $^{\circ}p < .001$. For the liver, sTRAIL MSCs vs CTR, EV MSCs or GD2 tCAR MSCs $*p < .001$, BF MSCs vs CTR, EV MSCs or GD2 tCAR MSCs $^{\circ}p < .001$. All p-values have been calculated using the Wilcoxon–Mann–Whitney test.

.05], and GD2 tCAR MSC [2.461 (0.797 to 3.318) vs 2.318 (1.182 to 3.202), 1.1-fold change; $p > .05$] groups (Fig. 6c). Differences in the levels of liver metastases between mice treated with BF MSCs and sTRAIL MSCs were not significant [1.375 (1.037 to 2.561) vs 2.461 (0.797 to 3.318), 0.6-fold change; $p > .05$; Fig. 6c]. However, based on the comparisons with control groups, the BF MSCs appeared to provide better control over tumour growth in the liver than sTRAIL MSCs, although without achieving significance (Fig. 6c). Collectively, these results suggested that the sTRAIL molecule produced in vivo by both sTRAIL and BF MSCs were able to significantly inhibit the growth of lung metastases.

GD2 tCAR improves the early targeting and retention of BF MSCs in the lungs

To investigate the MSC biodistribution and tumour-targeting efficiency, the last dose of MSCs was labelled with DiR dye before infusion. Nearly 100% of MSCs were effectively labelled following this protocol (Fig. 7a). DiR-labelled MSCs were followed for two days by IVIS, and the data were collected by applying fixed ROIs on the lungs and liver, which represented the primary organs affected by tumour growth and in which DiR fluorescence localised over time (Fig. 7b). As a free dye, DiR mainly localised to the liver (73.47% of total DiR fluorescence), with low lung retainment (14.55%) after i.v. injection (data not shown). Over time, the lung signal rapidly decreased, whereas fluorescence in the liver displayed a slower decline. When used to label MSCs, the biodistribution of DiR dye differed between treatment groups over time. At 4 h post-MSC injection, the fluorescence was equally distributed between the lungs and liver in EV MSC, GD2 tCAR MSC, and BF MSC groups ($p > .05$; Fig. 7c and d). In the sTRAIL MSC group, the hepatic signal was higher than the pulmonary signal [49.265% (45.965% to 51.546%) vs 36.428% (33.080% to 39.620%); $p < .005$; Fig. 7c and d]. Looking first at the lungs, as the first-pass mechanical barrier to systemic delivery, the expression of GD2 tCAR significantly improved the targeting of BF MSCs to lung metastases compared with sTRAIL MSCs [41.923% (38.879% to 45.617%) vs 36.983% (33.080% to 39.620%); $p < .05$; Fig. 7c, right panel]. In contrast to the pattern observed in the lungs, the BF MSC signal was significantly lower than that for sTRAIL MSCs in the liver [44.361% (41.092% to 47.849%) vs 48.877% (45.965% to 51.546%), respectively; $p < .05$ for all; Fig. 7d, right panel]. After 24 h, the signal in the lungs significantly decreased ($p < .05$; data not shown) while remaining stable in the liver ($p > .05$; data not shown) for all groups. BF MSC fluorescence showed a tendency towards increasing in the liver compared with the 4 h but failed to reach significance ($p > .05$; not shown). The overall trend observed for the lungs was similar to that seen after 4 h, with the BF MSC signal remaining higher than the sTRAIL MSC one, which approached significance ($p = .053$; data not shown). In the liver, BF MSC fluorescence became similar to that for sTRAIL MSCs [53.783% (51.907% to 54.754%) vs 55.574% (53.602% to 57.387%); $p > .05$; data not shown]. Two days after MSC injection, the distribution of DiR-labelled MSC fluorescence was comparable between the BF MSC and sTRAIL MSC groups, in both the lungs [19.811% (18.242% to 21.111%) vs 19.549% (18.520% to 21.384%); $p > .05$; data not shown] and the liver [57.672% (53.093% to 58.360%) vs 56.129% (53.379% to 57.873%); $p > .05$; data not shown]. The sTRAIL MSC and BF MSC fluorescence were lower in the lungs and higher in the liver compared with those in the EV and GD2 tCAR MSC groups ($p < .05$ for all comparisons; data not shown). Overall, these in vivo data indicated that the presence of the GD2 tCAR significantly improved the targeting and persistence of BF MSCs in the lungs at early time points. Despite the increase in the GD2 tCAR-mediated targeting of lung metastases, BF MSCs did not lose the ability to effectively localise to the liver, with levels comparable to sTRAIL MSCs at later time points.

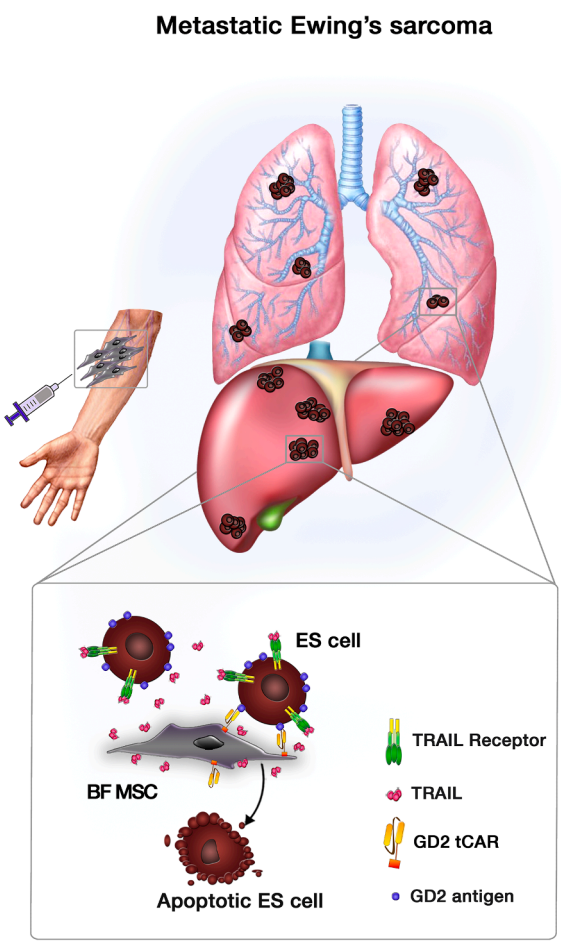

Fig. 8. BF MSC-based strategy for metastatic ES. Cartoon showing the putative targeted killing by intravenously injected BF MSCs expressing an artificial receptor against the GD2 (GD2 tCAR) and armed to constantly release a soluble variant of TRAIL (sTRAIL). GD2 tCAR was introduced to achieve the site-specific and prolonged retention of MSCs at ES metastatic sites (e.g., lungs) to provide the effective delivery of the TRAIL proapoptotic agent to the tumour. In the tumour, sTRAIL can exert its cytotoxic effects without requiring MSC contact with cancer cells, acting on both bound and nearby ES cells, regardless of GD2 expression.

BF MSCs effectively engraft to the lungs and liver in the ES metastatic model

While DiR labelling of MSCs revealed differences in their biodistribution associated with GD2 tCAR expression, DiR signal may become less specific due to previously described microenvironmental contamination [45]. Therefore, we wanted to further confirm the MSC engraftment in extracted organs using the highly sensitive control and sTRAIL 4-plex ddPCR assays. EV and GD2 tCAR MSCs were found to be equally present in the lungs [0.791 (0.565 to 0.865) vs 0.637 (0.478 to 0.747), 1.2-fold change; $p > .05$; Fig. 7e]. sTRAIL MSCs appeared to better persist into the lungs compared with BF MSCs, but this difference failed to reach significance [0.281 (0.230 to 0.352) vs 0.207 (0.116 to 0.259), 1.4-fold change; $p > .05$; Fig. 7e]. The retention of EV and GD2 tCAR MSCs in the lungs were significantly higher than the retention of sTRAIL and BF MSCs ($p < .05$; Fig. 7e). Compared with the lungs, higher numbers of sTRAIL and BF MSCs were detected in the liver (2.0- and 5.8-fold changes, respectively, $p < .05$; Fig. 7e and f), whereas EV and GD2 tCAR MSCs were nearly undetectable in the liver (Fig. 7f). In contrast to the trend observed in the lungs, BF MSCs appeared to double the level of sTRAIL MSCs in the liver, although this difference failed to achieve significance [1.200 (0.535 to 1.600) vs 0.523 (0.339 to 0.186),

2.3-fold change; $p > .05$; Fig. 7f]. Examining the ratio between the number of gene-modified MSCs and TC71 Luc tumour cells in the lungs, no differences were observed amonggroups ($p > .05$), and ratios were as follows: 5.774 (3.522 to 8.229) for the EV MSC group, 7.093 (2.918 to 10.717) for the GD2 tCAR MSC group, 7.674 (4.563 to 21.868) for the sTRAIL MSC group, and 5.730 (2.581 to 13.076) for the BF MSC group. In the liver, the ratio was negligible for both the EV and GD2 tCAR MSC groups, as MSCs were detected at extremely low levels in only a few mice. The ratios observed in the sTRAIL and BF MSC groups ($p < .001$) were significantly higher; tumour cells outnumber MSCs, resulting in similar ratios ($p > .05$) of 0.466 (0.099 to 1.002) and 0.698 (0.293 to 1.268), respectively. Overall, the ddPCR data confirmed that BF MSCs were able to effectively engraft to the lungs and liver in our ES metastatic model. By in vivo DiR fluorescence, we observed that the inclusion of GD2 tCAR assisted the targeting of BF MSCs to lung metastases during the first 24 h after MSC infusion. After three days, GD2 tCAR expression appeared to be advantageous for BF MSCs in terms of targeting and retention in the liver, where metastases were significantly more prominent than in the lung [1.375 (1.037 to 2.5661) vs 0.038 (0.021 to 0.058), 36.0-fold change; $p < .05$; Fig. 6b and c].

Discussion

We here originally demonstrated the possibility of counteracting metastatic ES using a CAR driven MSC approach, in which sTRAIL is delivered by MSCs expressing a surface anti-GD2 receptor, the GD2 tCAR (Fig. 8). The invasive nature of ES is an underlying cause for the failure of standard therapies [46]. The tumour-tropic ability of MSCs offers an alternative approach, in which these cells can be used as vehicles for the delivery of antitumour molecules [13]. MSCs are considered as putative cells of origin for ES and display an active role as progenitors of the tumour-supportive stroma [2,13,47]. To exploit these MSC features, our group successfully developed a therapeutic approach using MSCs as a vehicle for the delivery of proapoptotic TRAIL molecules, demonstrating that TRAIL MSCs have the capacity to infiltrate the ES microenvironment and destroy cancer from the inside, which is referred to as the Trojan horse effect [16,19]. Although a MSC-based delivery of TRAIL molecule has been established for primary localised ES [16,19], the therapeutic targeting of metastases remains challenging and has not yet been deeply investigated. We recently optimised the tumour affinity of MSCs expressing mTRAIL through the additional expression of an artificial receptor targeting the GD2 antigen, named BF MSCs [37]. GD2 is commonly expressed by ES and has been identified as a suitable antigen for immunotherapeutic approaches for the targeting of micrometastatic cells and the prevention of relapse [29]. In the current study, BF MSCs were armed to constantly release sTRAIL, for the development of a more powerful MSC-based therapeutic strategy for the treatment of metastatic ES. These BF MSCs combine a higher tumour affinity conferred by the expression of GD2 tCAR with the capacity to release sTRAIL, which can target even distant tumour cells, regardless of their GD2 expression levels.

The GD2 antigen and TRAIL receptor expression in ES cell lines were examined to predict both targeting affinity and TRAIL sensitivity. The examined ES cell lines could be distinguished as the GD2-higly positive TC71, the weakly GD2-positive A673 and the GD2-negative RD-ES. When TRAIL receptors were examined, FACS analyses revealed high levels of DR5 and low expression of DR4 for all lines, similar to the results reported by Picarda et al. [48]. The decoy receptor DcR1 was undetectable in all lines, whereas DcR2 was positively detected in TC71 cells with a low expression level in A673 cells, and undetectable in RD-ES. All cell lines were found to be sensitive to TRAIL-mediated apoptosis, with RD-ES cells showing the most sensitivity and TC71 cells displaying the most resistance, as previously described by Kontny et al. [49]. The inclusion of GD2 tCAR was able to improve the affinity of BF MSCs for ES cells, and the level of cell-to-cell interactions correlated with GD2-abundance in ES cell lines, as was previously reported for GBM [37]. In addition to enhancing binding specificity, the GD2 tCAR also enhanced the stability of the interaction between MSCs and GD2-higly positive TC71 cells. We then assessed the effectiveness of our cell therapy approach by examining the effects of BF MSCs against ES cells in both 2D and 3D co-cultures. In 2D co-cultures, all ES lines displayed strong sensitivity to BF MSCs, which resulted in tumour cell mortality levels comparable to those observed for sTRAIL MSCs and superior to rhTRAIL treatment in the TC71 line. sTRAIL-containing SN collected from BF MSCs was also able to induce significant cell death in all ES lines, comparable to the results obtained using sTRAIL MSC SN and rhTRAIL. However, the mean concentration of sTRAIL released by BF MSCs was approximately 4 000-fold less than the concentration used for rhTRAIL treatment. This might be explained by the superior stability and activity at 37 °C of the sTRAIL molecule versus the rhTRAIL, as previously reported against pancreatic cancer [17]. BF MSCs effectively killed TC71 and A673 cells in 3D spheroid models, with cytotoxicity equal to that observed for sTRAIL MSCs, confirming that the inclusion of GD2 tCAR did not affect the cytotoxic effects exerted by BF MSCs. Against the TC71 cell line, BF MSCs appeared to better activate the apoptotic pathway than rhTRAIL, further endorsing the advantage of using a cell-based strategy. TC71 cells were also seeded on a fibre-based matrix to model the tumour architecture and were allowed to reorganise into a 3D, in vivo-like tumour structure, similar to that established by Fong et al. [50]. Even at an unfavourable T:E ratio, BF MSCs were able to control tumour growth better than rhTRAIL and almost completely kill ES cells in 24 h. This assay originally revealed the advantage of using MSCs that constantly release sTRAIL over the application of rhTRAIL against ES, in line with the observations of several independent in vivo studies in which TRAIL MSCs displayed increased antitumour effects compared with rhTRAIL treatment [17,19].

These encouraging in vitro data indicated the improved tumour affinity and killing properties of BF MSCs to be further explored in an in vivo model of metastatic ES. Metastatic ES is a complex, heterogeneous disease that can present as solitary pulmonary or isolated bone metastasis or as a multiorgan-disseminated disease [6]. Individuals with widely disseminated ES constitute a high-risk group associated with a very dismal outcome [1,6]. Therefore, we felt the need to recreate an animal model mimicking that metastatic disease. In our NSG mouse-ES metastatic model the highly GD2-positive TC71 line, established from a metastatic ES [51], accumulated early in the lungs and then relocated to various sites, producing clear metastases as early as 10 days following injection. Almost 100% of transplanted mice developed tumours, with common engraftment sites including the lungs, liver, and bones, which closely mimics the severe clinical presentation observed in widely disseminated ES [1,6]. Despite pulmonary first-pass entrapment, tumours efficiently engrafted to the liver, where larger metastases were found compared with the lungs. To the best of our knowledge, this represents the first model with a very high rates of tumour engraftment in multiple metastatic sites obtained through the i.v. injection of the TC71 cell line. Metastases were rapidly detected by in vivo bioluminescence compared to other studies that infused higher number of cells [52–58]. To face this rapid spread of ES, treatment was started early after tumour injection by infusing multiple doses of BF MSCs since multiple metastatic sites and tumour growth heterogeneity might hamper the ability of BF MSCs to produce a detectable antitumour effect as a monotherapy. BF MSCs were able to counteract tumour growth in the lungs, resulting in the significant reduction of the tumour signal as detected by the sensitive ddPCR assay, which was similar to the pattern observed for sTRAIL MSCs. For metastases in the liver, only BF MSC treatment produced a slight, though not significant, antitumour effect compared with the control groups. Liver metastases in BF MSC-treated mice were reduced by 40% compared with sTRAIL MSC-treated mice, although this difference did not achieve significance. On contrary, EV and GD2 tCAR MSCs never affected tumour growth, presenting lung and liver metastases comparable to those observed for the CTR group. This finding contrasts with the data displayed by Hayes-Jordan et al., who

showed that i.v. injection of wild type rat bone marrow-derived MSCs decreased the volume of pulmonary metastatic lesions in an orthotopic chest wall model of ES [59].

The entrapment of MSCs in the lungs after systemic infusion makes them attractive vehicles for TRAIL delivery to ES lung metastases [23]. The physiological accumulation of cells in the lungs, combined with active tumour homing mechanisms, both control the MSC targeting of lung metastases after i.v. injection [36,60]. In our study, biological targeting of MSCs was further enhanced by the expression of GD2 tCAR on the MSC surface, which should favour MSC targeting and persistence at GD2-expressing tumour sites. To investigate the MSC biodistribution and tumour-targeting efficiency, the final delivery of gene-modified MSCs was labelled by DiR dye before infusion. While free DiR dye biodistribution after i.v. injection showed a primarily localization to the liver and a very low lung retention, DiR-labelled MSCs were clearly detected in lungs due to the partial cell entrapment after systemic injection. At early time points after infusion, the GD2 tCAR molecule significantly enhanced the targeting and persistence of BF MSCs in the lung, which represents the first-pass metastatic site. Even though metastases were reduced after the first and second MSC doses, the expression of GD2 tCAR conferred a tumour-binding advantage to BF MSCs over sTRAIL MSCs. The time window in which this difference was appreciable was relatively short (4–24 h after MSC injection) but generated an indication on the ability of BF MSCs to establish cell-to-cell interactions in vivo, resulting in a detectable increase in their retention in lung metastases compared with sTRAIL MSCs.

However, we believe that the GD2 tCAR-mediated targeting advantage of BF MSCs may not have lasted long enough to enable a better control of tumour growth in the lungs compared with sTRAIL MSCs. We can speculate that the BF MSC impact may last longer and result in a tumour killing advantage at higher doses based on more favourable T:E ratios. MSCs modified to express an AR against the erbB2 antigen showed a similar increased retention in the lungs compared with unmodified MSCs in an erbB2 transgenic mouse for up to 32 h after i.v injection [36]. Despite the increased retention in the lungs, BF MSCs did not lose the ability to effectively localise to the liver. At 24 h after MSC injection, BF MSCs showed a tendency to increase in the liver, and the in vivo signal became comparable to that detected for sTRAIL MSCs, especially after 48 h. After 3 days, animals were euthanised, and the MSC retention in the lungs and liver were ex vivo confirmed by ddPCR assays. We observed that as the amount of lung metastases changed in response to treatments, the number of MSCs engrafted to the lung varied accordingly, maintaining a relatively constant MSC to tumour cell ratio for all groups. In the sTRAIL and BF MSC groups, lung metastases were strongly reduced by the release of sTRAIL. Consequently, only a few sTRAIL and BF MSCs persisted in the lung, whereas the majority of MSCs migrated to the liver. In the liver, the tumour cells outnumbered the MSCs, and only the sTRAIL and BF MSCs were able to efficiently engraft and persist over time. Liver metastases were significantly more prominent than in the lung, and we can hypothesize that the inflammatory cytokines and chemokines released by tumour cells might play a role in the recruitment of MSCs to the liver [61]. BF MSCs appeared to be more present in the liver than sTRAIL MSCs, but this difference failed to reach significance due to the high variability between mice. After MSCs have homed to the liver, we can speculate that the tumour-targeting and retention of BF MSCs might have been improved by the expression of GD2 tCAR, which might also explain why liver metastases appeared to be slightly reduced in mice treated with BF MSCs. However, considering the unfavourable MSC to tumour cell ratio in the liver, we believe that those BF MSCs that were able to reach the liver had to cope with too large metastases to produce a significant antitumour effect. Overall, the expression of GD2 tCAR appeared to strengthen the binding of MSCs to metastases, resulting in an increase in the tumour-associated MSC signal which was detected early in the lungs. At later time points, we observed a tendency of GD2 tCAR to improve the retention of BF MSCs in the liver.

In the past, cellular therapy strategies based on CAR-modified T or NK cells applied as monotherapy have failed to control tumour growth in different metastatic models of ES [31,32]. The synergistic inhibition of metastatic disease has been achieved through the combination of anti-GD2 CAR T cell therapy with an HGF receptor-neutralising antibody, with the intent to reduce tumour burden creating a more favourable microenvironment for immunotherapy [34]. Based on very encouraging in vitro findings, our work represents a first attempt to in vivo treat widely disseminated ES using MSCs that have been genetically modified to deliver an anticancer molecule in combination with a tCAR. With the limitation of a monotherapy approach, we provided preliminary insights on the potential effects of BF MSCs within a complex ES metastatic model, additionally exploring MSCs biodistribution. These results warrant further investigations regarding the optimal cell dose and schedule, together with the possibility of introducing combinatory approaches with other anticancer agents, as we demonstrated against pancreatic cancer [18]. Overall, the BF MSC-based strategy promises to pave the way for potential improvements in the therapeutic delivery of TRAIL proapoptotic molecules for the treatment of ES and other deadly GD2-positive malignancies.

Contributors

GGo: Conception or design of the work, data collection, drafting the manuscript, data analysis, and interpretation, data finalization; MN, AC, LC: Data collection; GGr, MDa, GC, CS, RT, MP, CC, OC: Data collection, data analysis, and interpretation; FB, FR, RD: Data analysis and interpretation; MD: Conception or design of the work, drafting the manuscript, data analysis, interpretation and data finalization.

Data sharing statement

Materials used in this study are commercially available. Study-specific primary cell material can be provided upon availability and written request to the corresponding authors and signed material transfer agreement. Data can be made available upon request to the corresponding authors.

Declaration of Competing Interest

MD is the founder of Rigenerand Srl, a University start-up company developing gene therapy approaches for cancer. MD is also a member of the Board of Directors for Rigenerand Srl. MD's interests are managed by the University of Modena and Reggio Emilia in accordance with their conflicts of interest policies. GGr, MDa, CS and OC are currently employed by Rigenerand Srl. All other authors declare no competing interests. GGo, GGr, OC, CS and MD hold a patent related to the bifunctional technology.

Acknowledgements

Dr. Flavia Parise, Prof. Renata Battini and Dr. Antonella Mauro (Animal Facility, University of Modena & Reggio Emilia) for technical support in the development of pre-clinical in vivo data. Dr. Lara Rossini (Field Application Specialist, Bio-Rad) for the technical support in the setting of the ddPCR assays. This work was supported in part by: Associazione Italiana Ricerca Cancro (AIRC) grant IG 2015 #17326 (MD) and Project "Dipartimenti Eccellenti MIUR 2017" (MD, GGr). GGo was supported by a AIRC fellowship for Italy (#226439), CC is assignee of the Diana Laneri Post-Doctoral Fellowship. sTRAIL vector has been generously made available by Rigenerand Srl.

Supplementary materials

Supplementary material associated with this article can be found, in the online version, at doi:10.1016/j.tranon.2021.101240.

References

[1] D.L. Casey, T.-.Y. Lin, N.-.K.V. Cheung, Exploiting signaling pathways and immune targets beyond the standard of care for Ewing sarcoma, Front Oncol 9 (2019) 537.
[2] N. Riggi, M.-.L. Suva, I. Stamenkovic, Ewing's sarcoma origin: from duel to duality, Expert Rev Anticancer Ther 9 (8) (2009) 1025–1030.
[3] S.L. Lessnick, M. Ladanyi, Molecular pathogenesis of ewing sarcoma: new therapeutic and transcriptional targets, Ann. Rev. Pathol. Mech. Dis. 7 (1) (2012) 145–159.
[4] R. Ladenstein, U. Pötschger, M.C. Le Deley, J. Whelan, M. Paulussen, O. Oberlin, et al., Primary disseminated multifocal ewing sarcoma: results of the euro-ewing 99 trial, J. Clin. Oncol. 28 (20) (2010) 3284–3291.
[5] N. Gaspar, D.S. Hawkins, U. Dirksen, I.J. Lewis, S. Ferrari, M.-.C. Le Deley, et al., Ewing sarcoma: current management and future approaches through collaboration, J. Clin. Oncol. 33 (27) (2015) 3036–3046.
[6] N. Khanna, A. Pandey, J. Bajpai, Metastatic Ewing's sarcoma: revisiting the "evidence on the fence, Indian J. Med. Paediatr. Oncol. Off. J. Indian Soc. Med. Paediatr. Oncol. 38 (2) (2017) 173–181.
[7] T.G.P. Grünewald, F. Cidre-Aranaz, D. Surdez, E.M. Tomazou, E. de Álava, H. Kovar, et al., Ewing sarcoma, Nat. Rev. Dis. Primer 4 (1) (2018) 5.
[8] A. Ashkenazi, P. Holland, S.G. Eckhardt, Ligand-based targeting of apoptosis in cancer: the potential of recombinant human apoptosis ligand 2/tumor necrosis factor–related apoptosis-inducing ligand (rhApo2L/TRAIL), J. Clin. Oncol. 26 (21) (2008) 3621–3630.
[9] A.-.L. Kretz, A. Trauzold, A. Hillenbrand, U. Knippschild, D. Henne-Bruns, S. von Karstedt, et al., TRAILblazing strategies for cancer treatment, Cancers (Basel) 11 (4) (2019) 456.
[10] S. von Karstedt, A. Montinaro, H. Walczak, Exploring the TRAILs less travelled: TRAIL in cancer biology and therapy, Nat. Rev. Cancer 17 (6) (2017) 352–366.
[11] H. Dianat-Moghadam, M. Heidarifard, A. Mahari, M. Shahgolzari, M. Keshavarz, M. Nouri, et al., TRAIL in oncology: from recombinant TRAIL to nano- and self-targeted TRAIL-based therapies, Pharmacol Res 155 (2020), 104716.
[12] G. Grisendi, C. Spano, F. Rossignoli, N. D Souza, G. Golinelli, A. Fiori, et al., Tumor stroma manipulation by MSC, Curr. Drug Targets 17 (10) (2016) 1111–1126.
[13] G. Golinelli, I. Mastrolia, B. Aramini, V. Masciale, M. Pinelli, L. Pacchioni, et al., Arming mesenchymal stromal/stem cells against cancer: has the time come? Front. Pharmacol. 11 (2020), 529921.
[14] G. Grisendi, R. Bussolari, L. Cafarelli, I. Petak, V. Rasini, E. Veronesi, et al., Adipose-derived mesenchymal stem cells as stable source of tumor necrosis factor-related apoptosis-inducing ligand delivery for cancer therapy, Cancer Res. 70 (9) (2010) 3718–3729.
[15] G. Golinelli, G. Grisendi, C. Spano, M. Dominici, Surrounding pancreatic adenocarcinoma by killer mesenchymal stromal/stem cells, Hum. Gene. Ther. 25 (5) (2014) 406–407.
[16] G. Grisendi, C. Spano, N. D'souza, V. Rasini, E. Veronesi, M. Prapa, et al., Mesenchymal progenitors expressing TRAIL induce apoptosis in sarcomas: adipose MSC with TRAIL target sarcomas, Stem Cells 33 (3) (2015) 859–869.
[17] C. Spano, G. Grisendi, G. Golinelli, F. Rossignoli, M. Prapa, M. Bestagno, et al., Soluble TRAIL armed human MSC as gene therapy for pancreatic cancer, Sci Rep 9 (1) (2019), 1788.
[18] F. Rossignoli, C. Spano, G. Grisendi, E.M. Foppiani, G. Golinelli, I. Mastrolia, et al., MSC-delivered soluble TRAIL and paclitaxel as novel combinatory treatment for pancreatic adenocarcinoma, Theranostics 9 (2) (2019) 436–448.
[19] R. Guiho, K. Biteau, G. Grisendi, J. Taurelle, M. Chatelais, M. Gantier, et al., TRAIL delivered by mesenchymal stromal/stem cells counteracts tumor development in orthotopic Ewing sarcoma models: MSC-TRAIL counteract-Ewing sarcoma tumor development, Int. J. Cancer 139 (12) (2016) 2802–2811.
[20] T.J. Kean, P. Lin, A.I. Caplan, J.E. Dennis, MSCs: delivery routes and engraftment, cell-targeting strategies, and immune modulation, Stem Cells Int. 2013 (2013) 1–13.
[21] J. Gao, J.E. Dennis, R.F. Muzic, M. Lundberg, A.I. Caplan, The dynamic in vivo distribution of bone marrow-derived mesenchymal stem cells after infusion, Cells Tissues Organs 169 (1) (2001) 12–20.
[22] S. Schrepfer, T. Deuse, H. Reichenspurner, M.P. Fischbein, R.C. Robbins, M. P. Pelletier, Stem cell transplantation: the lung barrier, Transplant Proc 39 (2) (2007) 573–576.
[23] M. Salvadori, N. Cesari, A. Murgia, P. Puccini, B. Riccardi, M. Dominici, Dissecting the pharmacodynamics and pharmacokinetics of MSCs to overcome limitations in their clinical translation, Mol. Ther. - Methods Clin. Dev. 14 (2019) 1–15.
[24] A. Brooks, K. Futrega, X. Liang, X. Hu, X. Liu, D.H.G. Crawford, et al., Concise review: quantitative detection and modeling the in vivo kinetics of therapeutic mesenchymal stem/stromal cells: detection and modeling kinetics of stem cells, Stem Cells Transl. Med. 7 (1) (2018) 78–86.
[25] M. Prapa, S. Caldrer, C. Spano, M. Bestagno, G. Golinelli, G. Grisendi, et al., A novel anti-GD2/4-1BB chimeric antigen receptor triggers neuroblastoma cell killing, Oncotarget 6 (28) (2015) 24884–24894.
[26] B. Nazha, C. Inal, T.K. Owonikoko, Disialoganglioside GD2 expression in solid tumors and role as a target for cancer therapy, Front Oncol 10 (2020) 1000.
[27] M. Lipinski, K. Braham, I. Philip, J. Wiels, T. Philip, C. Goridis, et al., Neuroectoderm-associated antigens on Ewing's sarcoma cell lines, Cancer Res. 47 (1) (1987) 183–187.
[28] H.R. Chang, C. Cordon-Cardo, A.N. Houghton, N.K. Cheung, M.F. Brennan, Expression of disialogangliosides GD2 and GD3 on human soft tissue sarcomas, Cancer 70 (3) (1992) 633–638.
[29] S. Kailayangiri, B. Altvater, J. Meltzer, S. Pscherer, A. Luecke, C. Dierkes, et al., The ganglioside antigen GD2 is surface-expressed in Ewing sarcoma and allows for MHC-independent immune targeting, Br. J. Cancer 106 (6) (2012) 1123–1133.
[30] G. Dotti, S. Gottschalk, B. Savoldo, M.K. Brenner, Design and development of therapies using chimeric antigen receptor-expressing T cells, Immunol. Rev. 257 (1) (2014) 107–126.
[31] L. Liebsch, S. Kailayangiri, L. Beck, B. Altvater, R. Koch, C. Dierkes, et al., Ewing sarcoma dissemination and response to T-cell therapy in mice assessed by whole-body magnetic resonance imaging, Br. J. Cancer 109 (3) (2013) 658–666.
[32] S. Kailayangiri, B. Altvater, C. Spurny, S. Jamitzky, S. Schelhaas, A.H. Jacobs, et al., Targeting Ewing sarcoma with activated and GD2-specific chimeric antigen receptor-engineered human NK cells induces upregulation of immune-inhibitory HLA-G, Oncoimmunology 6 (1) (2017), e1250050.
[33] C. Spurny, S. Kailayangiri, B. Altvater, S. Jamitzky, W. Hartmann, E. Wardelmann, et al., T cell infiltration into Ewing sarcomas is associated with local expression of immune-inhibitory HLA-G, Oncotarget 9 (5) (2018) 6536–6549.
[34] M. Charan, P. Dravid, M. Cam, A. Audino, A.C. Gross, M.A. Arnold, et al., GD2-directed CAR-T cells in combination with HGF-targeted neutralizing antibody (AMG102) prevent primary tumor growth and metastasis in Ewing sarcoma, Int. J. Cancer 146 (11) (2020 Jun) 3184–3195.
[35] I.V. Balyasnikova, R. Franco-Gou, J.M. Mathis, M.S. Lesniak, Genetic modification of mesenchymal stem cells to express a single-chain antibody against EGFRvIII on the cell surface, J. Tissue Eng. Regen. Med. 4 (4) (2010) 247–258.
[36] S. Komarova, J. Roth, R. Alvarez, D.T. Curiel, L. Pereboeva, Targeting of mesenchymal stem cells to ovarian tumors via an artificial receptor, J. Ovarian Res. 3 (2010) 12.
[37] G. Golinelli, G. Grisendi, M. Prapa, M. Bestagno, C. Spano, F. Rossignoli, et al., Targeting GD2-positive glioblastoma by chimeric antigen receptor empowered mesenchymal progenitors, Cancer Gene Ther [Internet] (2018) [cited 2019 Aug 7]; Available from, http://www.nature.com/articles/s41417-018-0062-x.
[38] F. Rossignoli, G. Grisendi, C. Spano, G. Golinelli, A. Recchia, G. Rovesti, et al., Inducible Caspase9-mediated suicide gene for MSC-based cancer gene therapy, Cancer Gene. Ther. (2018).
[39] J.C. Marx, J.A. Allay, D.A. Persons, S.A. Nooner, P.W. Hargrove, P.F. Kelly, et al., High-efficiency transduction and long-term gene expression with a murine stem cell retroviral vector encoding the green fluorescent protein in human marrow stromal cells, Hum. Gene Ther. 10 (7) (1999) 1163–1173.
[40] A. López-Requena, C. Mateo de Acosta, M. Bestagno, A.M. Vázquez, R. Pérez, O. R Burrone, Gangliosides, Ab1 and Ab2 antibodies IV. Dominance of VH domain in the induction of anti-idiotypic antibodies by gene gun immunization, Mol. Immunol. 44 (11) (2007) 3070–3075.
[41] O. Candini, G. Grisendi, E.M. Foppiani, M. Brogli, B. Aramini, V. Masciale, et al., A novel 3D in vitro platform for pre-clinical investigations in drug testing, Gene. Ther. Immunol. Sci. Rep.. 9 (1) (2019), 7154.
[42] C. Maletzki, S. Bock, P. Fruh, K. Macius, A. Witt, F. Prall, et al., NSG mice as hosts for oncological precision medicine, Lab Invest. 100 (1) (2020) 27–37.
[43] F.G. Giancotti, Mechanisms governing metastatic dormancy and reactivation, Cell 155 (4) (2013) 750–764.
[44] M. Bernstein, H. Kovar, M. Paulussen, R.L. Randall, A. Schuck, L.A. Teot, et al., Ewing's sarcoma family of tumors: current management, Oncologist 11 (5) (2006) 503–519.
[45] F. Lassailly, E. Griessinger, D. Bonnet, Microenvironmental contaminations" induced by fluorescent lipophilic dyes used for noninvasive in vitro and in vivo cell tracking, Blood 115 (26) (2010) 5347–5354.
[46] D. Van Mater, L. Wagner, Management of recurrent Ewing sarcoma: challenges and approaches, OncoTargets Ther. Volume 12 (2019) 2279–2288.
[47] G. Grisendi, R. Bussolari, E. Veronesi, S. Piccinno, J.S. Burns, G. De Santis, et al., Understanding tumor-stroma interplays for targeted therapies by armed mesenchymal stromal progenitors: the Mesenkillers, Am. J. Cancer Res. 1 (6) (2011) 787–805.
[48] G. Picarda, F. Lamoureux, L. Geffroy, P. Delepine, T. Montier, K. Laud, et al., Preclinical evidence that use of TRAIL in Ewing's sarcoma and osteosarcoma therapy inhibits tumor growth, prevents osteolysis, and increases animal survival, Clin. Cancer Res. 16 (8) (2010) 2363–2374.
[49] H.U. Kontny, K. Hämmerle, R. Klein, P. Shayan, C.L. Mackall, C.M. Niemeyer, Sensitivity of Ewing's sarcoma to TRAIL-induced apoptosis, Cell Death Differ. 8 (5) (2001) 506–514.
[50] E.L.S. Fong, S.-.E. Lamhamedi-Cherradi, E. Burdett, V. Ramamoorthy, A.J. Lazar, F. K. Kasper, et al., Modeling Ewing sarcoma tumors in vitro with 3D scaffolds, Proc. Natl. Acad. Sci. 110 (16) (2013) 6500–6505.
[51] W.A. May, R.S. Grigoryan, N. Keshelava, D.J. Cabral, L.L. Christensen, J. Jenabi, et al., Characterization and drug resistance patterns of Ewing's sarcoma family tumor cell lines, Castresana JS, editor. PLoS ONE 8 (12) (2013) e80060.
[52] K. Scotlandi, S. Benini, M.C. Manara, M. Serra, P. Nanni, P.-.L. Lollini, et al., Murine model for skeletal metastases of Ewing's sarcoma, J. Orthop. Res. 18 (6) (2000) 959–966.
[53] S. Hu-Lieskovan, J.D. Heidel, D.W. Bartlett, M.E. Davis, T.J. Triche, Sequence-specific knockdown of EWS-FLI1 by targeted, nonviral delivery of small interfering rna inhibits tumor growth in a murine model of metastatic Ewing's sarcoma, Cancer Res 65 (19) (2005) 8984–8992.
[54] M. Hatano, Y. Matsumoto, J. Fukushi, T. Matsunobu, M. Endo, S. Okada, et al., Cadherin-11 regulates the metastasis of Ewing sarcoma cells to bone, Clin. Exp. Metastasis 32 (6) (2015) 579–591.
[55] K. von Heyking, J. Calzada-Wack, S. Göllner, F. Neff, O. Schmidt, T. Hensel, et al., The endochondral bone protein CHM1 sustains an undifferentiated, invasive

phenotype, promoting lung metastasis in Ewing sarcoma, Mol. Oncol. 11 (9) (2017) 1288–1301.
[56] J. Vormoor, G. Baersch, S. Decker, M. Hotfilder, K.L. Schäfer, L. Pelken, et al., Establishment of an in vivo model for pediatric Ewing tumors by transplantation into NOD/scid mice, Pediatr Res. 49 (3) (2001) 332–341.
[57] T. Schluep, Preclinical efficacy of the camptothecin-polymer conjugate IT-101 in multiple cancer models, Clin. Cancer Res. 12 (5) (2006) 1606–1614.
[58] A.K. Ikeda, D.R. Judelson, N. Federman, K.B. Glaser, E.M. Landaw, C.T. Denny, et al., ABT-869 inhibits the proliferation of ewing sarcoma cells and suppresses platelet-derived growth factor receptor and c-KIT signaling pathways, Mol. Cancer Ther. 9 (3) (2010) 653–660.
[59] A. Hayes-Jordan, Y.X. Wang, P. Walker, C.S. Cox, Mesenchymal stromal cell dependent regression of pulmonary metastasis from Ewing's, Front. Pediatr. 2 (2014) [Internet][cited 2021 Jun 7]Available from: http://journal.frontiersin.org/article/10.3389/fped.2014.00044/abstract.
[60] T.E.G. Krueger, D.L.J. Thorek, S.R. Denmeade, J.T. Isaacs, W.N. Brennen, Concise review: mesenchymal stem cell-based drug delivery: the good, the bad, the ugly, and the promise: MSC-based drug delivery: good, bad, ugly, & promise, Stem Cells Transl. Med. 7 (9) (2018) 651–663.
[61] N. D'souza, J.S. Burns, G. Grisendi, O. Candini, E. Veronesi, S. Piccinno, et al., MSC and tumors: homing, differentiation, and secretion influence therapeutic potential, Adv. Biochem. Eng. Biotechnol. 130 (2013) 209–266.